

Bahria University


Department of Earth & Environmental Sciences

Islamabad Campus, Islamabad

Dated: 06/12/2021

Certificate

A thesis submitted by **Ms. Aiza Amjad** to the Department of Earth & Environmental Sciences, Bahria University, Islamabad in partial fulfillment of the requirements for the degree of **Masters in Geophysics** (Session **2019-2021**).

Committee Member	Name	Signature
Supervisor	Ms. Urooj Shakir	
Co-Supervisor	Dr. Muhammad Shahid Riaz	
Internal Examiner	Mr. M. Raiees Amjad	
External Examiner	Dr. Abid Ali	
Post Graduate Coordinator	Dr. Muhsan Ehsan	
Head of Department (E&ES)	Dr. Said Akbar Khan	

**STATIC EARTHQUAKE TRIGGERING AND SEISMIC
HAZARD ASSESSMENT OF SULAIMAN LOBE,
CENTRAL INDUS BASIN, PAKISTAN**



AIZA AMJAD

01-262192-021

A thesis submitted to Bahria University, Islamabad in partial fulfillment of the requirement for the degree of M.S in Geophysics

Department of Earth and Environmental Sciences

Bahria University, Islamabad

2021

ACKNOWLEDEMENT

First, I am grateful to Allah S.W.T, the Almighty, for giving me this opportunity and strength to complete my thesis. I would like to sincerely thank you my supervisor Miss Urooj, Senior Assistant Professor, Department of Earth and Environmental sciences, Bahria University Islamabad and my Co-supervisor, Dr. Muhammad Shahid Riaz, Principal Scientist (Centre for Earthquake Studies, National Centre for Physics). He has been there providing his full support and excellent guidance at all times and has given me inspiration and suggestions during my studies. His guidance helped me in all the time of research and writing of this thesis. I feel very honoured that the Centre for Earthquake Studies (NCP) has provided me with an opportunity to work under their great environment. I am thankful to Dr. Muhammad Ali Shah, Director CES, for his administrative support.

I wish to express my sincere thanks to all of the Department faculty members for their continuous encouragement, support and attention.

I would like to save the last paragraph to thank my family and loved ones. I want to thank my parents for understanding, praying and supporting me during my study. I would never have succeeded without my family. Last but not least I would like to express my gratitude to everyone who has helped me with my project at any stage.

ABSTRACT

The purpose of this study is the seismic hazard assessment of Sulaiman lobe, Central Indus Basin, Pakistan. The curve-shaped Chaman transform fault, ~1000km long, the major active fault between Pakistan and Afghanistan demarks the western boundary of the Indian plate. Many catastrophic earthquakes have been occurred in this region. Until now, very few studies have been conducted to ascertain the earthquakes/fault interaction and hazard assessment for this region. By employing the stress triggering theory, an earthquake sequence, comprising of fifteen earthquakes occurred in the study region since 1888 is studied. Our findings reveal that eight out of fifteen earthquakes are triggered by the preceding earthquakes. The 1908, 1910, 1935, 1966, 1997 of magnitudes Mw 6.3, 6.2, 7.4, 6.2, 7.1 respectively are somewhat independent earthquakes in this sequence. The 1935 earthquake significantly increased the positive stress at both ends of its rupture. Later, the 1975 earthquake with ΔCFS above the triggering threshold value, and the 1990 earthquake occurred on the Ghazaband fault in the southern positive lobe. Since 1935 earthquake significantly increased the ΔCFS at both ends of the rupture, the 2008 Ziarat doublet earthquakes with magnitude Mw 2008 occurred on the Urghargai fault in the northern positive stress lobe where ΔCFS is positive. Furthermore, the northern segment of Chaman fault, southern segment of the Ghazaband fault and the northwestern segment of the Urghargai fault demonstrates a high value ΔCFS . It has the potential to cause seismicity in these areas necessitating plans to prevent any future seismic hazards. The seismic hazard maps indicated that some areas needed to be studied more thoroughly due to the hazard levels expected there. This research work aims to improve our understanding of earthquake triggering and fault interaction in the area of interest. For future work, an improved CFS maps related to earthquake triggering may be produced by incorporating definite lithospheric dynamics which requires instrumental data investigations for the area being studied.

CONTENTS

CHAPTER	TITLE	PAGE
	ACKNOWLEDEMENT	i
	ABSTRACT	ii
	TABLE OF CONTENTS	iii
	LIST OF FIGURES	vii
	LIST OF TABLES	viii
1	INTRODUCTION	1
	1.1 Overview	1
	1.2 Location of Study area	2
	1.3 Previous work	3
	1.4 Aims of the study	5
	1.5 Methodology	6
	1.6 Dataset	7
2	TECTONICS AND SEISMICITY OF STUDY AREA	8
	2.1 Regional setting	8
	2.2 Sedimentary basin of Pakistan	8
	2.3 Indus Basin Geologic history	8
	2.4 Central Indus Basin	9
	2.5 Tectonic setting	9
	2.6 Geological setting	11
	2.7 Stratigraphic sequence of sulaiman lobe	12
	2.8 Seismicity of study area	12
3	EARTHQUAKE CATALOGUE ANALYSIS AND DATA	

	PRE-PROCESSING	15
	3.1 Introduction	15
	3.2 Data sources	15
	3.3 Earthquake parameters calculation	16
	3.3.1 The 1888 Quetta Earthquake (M=6.3)	18
	3.3.2 The 1892 Chaman Earthquake (M=6.5)	18
	3.3.3 The 1893 Quetta Earthquake (M=6.0)	18
	3.3.4 The 1900 Earthquake (M=6.1)	18
	3.3.5 The 1908 Earthquake (M=6.3)	18
	3.3.6 The 1910 Earthquake (M=6.2)	19
	3.3.7 Mach Earthquake 1931 (M=7.3)	19
	3.3.8 The Quetta Earthquake 1935 (M=7.7)	19
	3.3.9 The 1966 Duki Earthquake (M=6.2)	19
	3.3.10 The 1975 Earthquake (M=6.8, 6.6)	19
	3.3.11 The 1990 Earthquake (M=6.2)	20
	3.3.12 Balochistan Earthquake 1997 (M=7.1)	20
	3.3.13 Ziarat Doublet Earthquakes (M=6.4)	20
4	METHODOLOGY FOR STRESS COMPUTATION	22
	4.1 Introduction	22
	4.2 Model and methods	22
	4.2.1 Calculation of coulomb stress changes	22
	4.2.2 Multilayered lithospheric model	23
	4.3 Computation of Green function using FORTRAN77 program "PSGRN"	24
	4.3.1 Parameters for Green function input file	25
	4.3.2 Parameters for output file	26
	4.4 Computation of stresses using FORTRAN77 program "PSCMP"	27
	4.4.1 Parameters for stresses computation input	

	file	27
5	RESULTS AND DISCUSSION	30
5.1	Numerical results and analysis	30
5.1.1	Co- and post-seismic stress changes (M 6.3 1888 earthquake)	30
5.1.2	Co- and post-seismic stress changes (M 6.5 1892 earthquake)	31
5.1.3	Co- and post-seismic stress changes (M 6.0 1893 earthquake)	32
5.1.4	Co- and post-seismic stress changes (M 6.1 1900 earthquake)	33
5.1.5	Co- and post-seismic stress changes (M=6.3 1908 earthquake)	33
5.1.6	Co- and post-seismic stress changes (M 6.2 by 1910 earthquake)	34
5.1.7	Co- and post-seismic stress changes (M=7.2 1931 earthquake)	35
5.1.8	Co- and post-seismic stress changes (M=7.4 1935 earthquake)	36
5.1.9	Co- and post-seismic stress changes (M=6.2 1966 earthquake)	37
5.1.10	Co- and post-seismic stress changes (M=6.8 1975a earthquake)	38
5.1.11	Co- and post-seismic stress changes (M=6.6 1975b earthquake)	38
5.1.12	Co- and post-seismic stress changes (M=6.2 1990 earthquake)	39

5.1.13	Co- and post-seismic stress (M=7.1 1997 earthquake)	40
5.1.14	Co- and post-seismic stress changes (M=6.4 2008a and 2008b earthquake)	41
5.2	Robustness of results	45
5.2.1	Co-efficient of friction	45
5.2.2	Viscosity	45
	CONCLUSIONS	64
	REFERENCES	66

FIGURES

FIGURE NO.	TITLE	PAGE
Figure 1.1.	Location map of study area	3
Figure 1.2.	Workflow for seismic hazard analysis	6
Figure 2.1.	Seismotectonic map of study area	14
Figure 2.5.	Geographic and tectonic setting of Sulaiman lobe and Range	11
Figure 3.1	Location map of all 15 selected earthquakes	21
Figure 4.1	Input file parameters	29
Figure 5.1.	The Coseismic Coulomb stress changes caused by the 1888-2008 earthquake ($\mu' = 0.4$, $\eta_{LC} = 1 \times 10^{18}$ Pa s $\eta_M = 1 \times 10^{19}$ Pa s)	44
Figure 5.2.	The Δ CFS evolution at the 10km depth since 1888 (post-seismic) ($\mu' = 0.4$, $\eta_{LC} = 1 \times 10^{19}$ Pa s $\eta_M = 1 \times 10^{19}$ Pa s)	45
Figure 5.3.	The Δ CFS evolution at the 10km depth since 1888 ($\mu' = 0.2$, $\eta_{LC} = 1 \times 10^{18}$ Pa s $\eta_M = 1 \times 10^{18}$ Pa s)	48
Figure 5.4.	The Δ CFS evolution at the 10km depth since 1888 ($\mu' = 0.4$, $\eta_{LC} = 1 \times 10^{18}$ Pa s $\eta_M = 1 \times 10^{18}$ Pa s)	49
Figure 5.5.	The Δ CFS evolution at the 10km depth since 1888 ($\mu' = 0.6$, $\eta_{LC} = 1 \times 10^{18}$ Pa s $\eta_M = 1 \times 10^{18}$ Pa s)	50
Figure 5.6.	The Δ CFS evolution at the 10km depth since 1888 ($\mu' = 0.2$, $\eta_{LC} = 1 \times 10^{19}$ Pa s $\eta_M = 1 \times 10^{19}$ Pa s)	51
Figure 5.7.	The Δ CFS evolution at the 10km depth since 1888 ($\mu' = 0.6$, $\eta_{LC} = 1 \times 10^{19}$ Pa s $\eta_M = 1 \times 10^{19}$ Pa s)	52
Figure 5.8.	The Δ CFS evolution at the 10km depth since 1888 ($\mu' = 0.2$, $\eta_{LC} = 1 \times 10^{19}$ Pa s $\eta_M = 1 \times 10^{20}$ Pa s)	53
Figure 5.9.	The Δ CFS evolution at the 10km depth since 1888 ($\mu' = 0.4$, $\eta_{LC} = 1 \times 10^{19}$ Pa s $\eta_M = 1 \times 10^{20}$ Pa s)	54
Figure 5.10.	The Δ CFS evolution at the 10km depth since 1888 ($\mu' = 0.6$, $\eta_{LC} = 1 \times 10^{19}$ Pa s $\eta_M = 1 \times 10^{20}$ Pa s)	55

Figure 5.11.	The Δ CFS evolution at the 10km depth since 1888 ($\mu'= 0.2$, $\eta_{LC}= 1\times 10^{18}$ Pa s $\eta_M=1\times 10^{19}$ Pa s)	56
Figure 5.12.	The Δ CFS evolution at the 10km depth since 1888 ($\mu'= 0.4$, $\eta_{LC}= 1\times 10^{18}$ Pa s $\eta_M=1\times 10^{19}$ Pa s)	57
Figure 5.13.	The Δ CFS evolution at the 10km depth since 1888 ($\mu'= 0.6$, $\eta_{LC}= 1\times 10^{18}$ Pa s $\eta_M=1\times 10^{19}$ Pa s)	58
Figure 5.14.	The Δ CFS evolution at the 10km depth since 1888 ($\mu'= 0.2$, $\eta_{LC}= 1\times 10^{20}$ Pa s $\eta_M=1\times 10^{20}$ Pa s)	59
Figure 5.15.	The Δ CFS evolution at the 10km depth since 1888 ($\mu'= 0.4$, $\eta_{LC}= 1\times 10^{20}$ Pa s $\eta_M=1\times 10^{20}$ Pa s)	60
Figure 5.16.	The Δ CFS evolution at the 10km depth since 1888 ($\mu'= 0.6$, $\eta_{LC}= 1\times 10^{20}$ Pa s $\eta_M=1\times 10^{20}$ Pa s)	61
Figure 5.17	Hazard map of the study area	63

TABLES

TABLE NO.	TITLE	PAGE
Table 3.1.	Earthquake parameters calculation using empirical relation	17
Table 3.2.	Historical earthquakes in the studied area, as well as associated source parameters	17
Table 4.1.	Parameters of multilayered lithospheric model	24
Table 4.2.	Parameters for green function input file	25
Table 4.3.	Parameters for green function output file	26
Table 4.4.	Parameters for stresses computation output file	27
Table 5.1.	Simulation of results with various values of viscosity and friction	46

CHAPTER 1

INTRODUCTION

1.1 Overview

Humanity has been jolted by numerous natural and human disasters. Natural calamities i.e., eruption of volcanoes, flood cyclones, drought, forest fires, earthquakes and epidemic are well-known in different parts of our planet. The major contributors in natural disasters include earthquake events that results to loss of life, socio-economic disorder as well as the destruction of property. Over the years, these losses have developed due to increase in material resources and increase in population. The most powerful earthquakes have been known to cause massive damage and wipe out entire societies and nations (Ambraseys et al., 2004).

Pakistan is located in one of the most seismically active regions in the world, where the north-west moving Indian plate collides with the south-east moving Eurasian plate at a rate of around 1.7 inches per year (4.3 cm/yr.). The continental-continental collision is causing high seismic activity in the region. As a result of this collision, many mountain structures were formed such as Hindukush mountains, Pamir ranges, Kirthar and Sulaiman ranges and Karakorum mountains. The Sulaiman Mountains is a north-south extension of the Hindukush mountain system. The highest peak of the range is Zarghun Ghar which is 3,578 metres (11,739 ft) and is located near Quetta, Pakistan. The kirthar mountains are a mountain range that marks the boundary between the Pakistan provinces of Sindh and Balochistsn. Large, frequently devastating earthquakes occurred by the slip of the major faults caused due to this collision (Sultan, 2015). Some examples of devastating earthquakes are mentioned below:

1. On October 8, 2005, a M 7.5 earthquake struck Kashmir, Pakistan, killing over 80,000 individuals and assessing five million people homeless.

2. Another earthquake occurred on Oct 29, 2008 in Quetta, Pakistan of M 6.4 killing beyond 10,000 people, assessing 0.5 million people destitute and the
3. Great 2013 Awaran Earthquake of M 7.7 which caused more than 825 fatalities.

The stress changes related with a seismic tremor define the mechanism of earthquake triggering, which can promote or delay seismic activity in the vicinity or trigger further tremors at a greater distance. This mechanism is the outcome of stresses redistribution induced by an earthquake. However, overall function of the earthquake is to relieve the elastic stress accumulated in the crust where these stresses actually are increased due to the occurrence of coseismic fault slip (Freed, 2005). Earthquakes are caused by the stress changes of 0.01 MPa which are enough to trigger seismicity.

Static triggering can be used for different studies i.e., co-seismic, seismic hazard point of view, earthquake triggering point of view (major inter-event) etc. Geophysicists seek to assess earthquakes and their associated uncertainties through Seismic Hazard Assessment. Natural or man-made events i.e., earthquakes or hurricanes have unique positions in time and space (Wang, 2011).

Seismological and geological studies provide the extensive information about the earthquake events along with their parameters. Static earthquake triggering is an important approach for studying the relationship between the earthquakes and as a result, determining the seismic hazard in an area of interest. The study area has been subjected to this methodology which includes the calculation of stresses due to earthquake owing to static earthquake triggering and then generating stress maps which helped us to delineate vulnerable areas that are useful for hazard assessment.

1.2 Location of study area

Sulaiman Lobe is a part of the Sulaiman Range, which is a north–south extension of the southern Hindu Kush Mountain system that rises to form eastern edge of the Iranian plateau and the northeastern edge of the Baluchistan Plateau. They are located in the Zabul, Kandahar and Loya Paktia regions of Afghanistan whereas in Pakistan they extend to northern Baluchistan and some parts of southwestern Khyber Pakhtunkhwa and Punjab (Jadoon, 1991). The coordinates of study area lie between 27-32° N and 66-72°E. It covers an area of 2,172.89 square kilometers and is located in the Zhob, Killa, Musakhel, Saifullah and Loralai regions of Baluchistan Province, Pakistan.

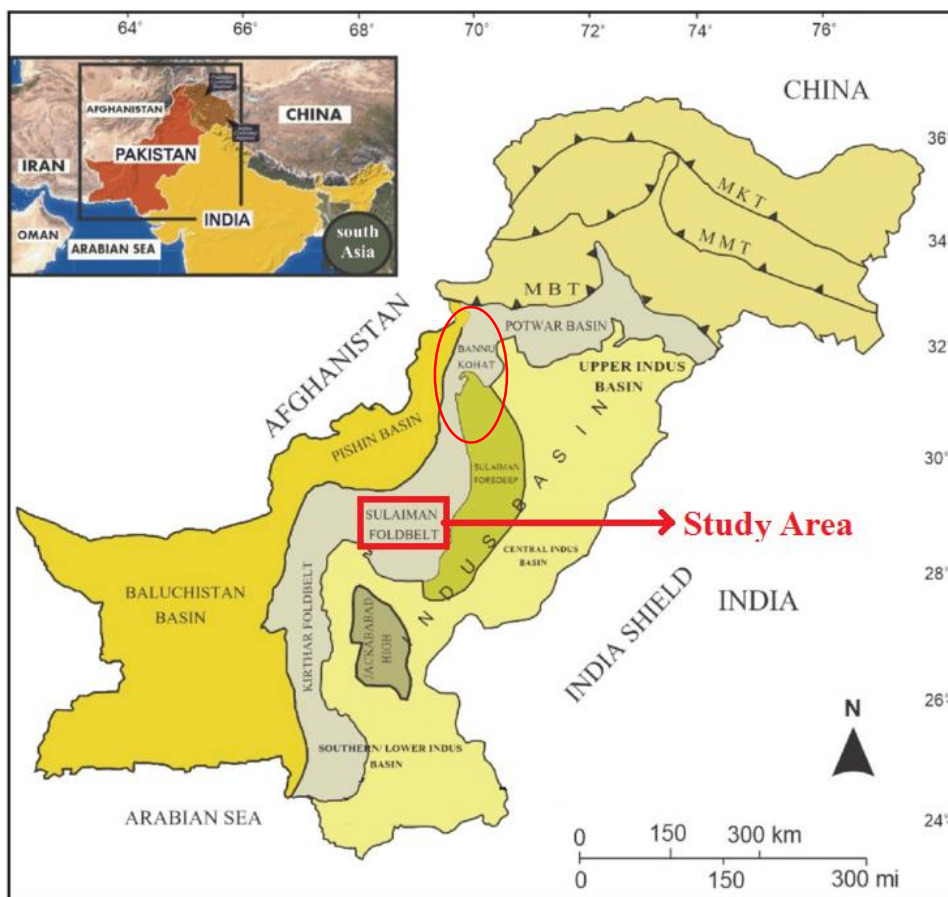


Figure 1.1. Location map of study area (Jan and Kazmi, 1997)

1.3 Previous work

(Blanford, 1883) and (Oldham, 1890) completed early exploration work in the Sulaiman Range (Eames et al., 1952). (Davies, 1940) and (Pinfold, 1939) conducted stratigraphic and paleogeographic studies of Cretaceous/Paleocene rocks in the Sulaiman Range. On the Sulaiman Range's eastern side, (Eames et al., 1952) focused on the core stratigraphy of Zindapir as well as Fort Munro structures (Jones, 1961).

(Abdel, 1971) and (Rowland, 1978) used satellite pictures to assess the shape and general structure of the Sulaiman lobe. At scale i.e 1:250,000, Kidwai and Hemphill in 1973 surveyed the northern section of the Sulaiman Range and discovered multiple strike-slip and thrust faults. The arcuate shape of sulaiman lobe was interpreted by (Sarwar et al., 1979).

(Gansser, 1979), (Abbas et al., 1979) and (Allemann, 1979) have all detailed the various peculiarities of the ophiolites from the Zhob valley. (Malik et al., 1988) reviewed the Sulaiman foredeep oil and gas potential and prospects.

Using gravity modelling and comparing the thickness of a sequence of platforms between the Sulaiman and Salt ranges, the potential of a thin transitional crust/oceanic crust beneath the Sulaiman Range was studied (Lillie et al., 1989). Oil companies such as HDIP, GSP, OGDCL etc have done a lot of work in the Sulaiman range.

The presence of active faults and an extreme degree of seismicity suggest active deformation of the Sulaiman region (Quittmeyer et al., 1979). Sulaiman fold belt exposes strata from the recent (0 Ma) to the Permo-Triassic Alzoi Group (284 Ma). The formation thickness in front of the mountain is about 10km (Jadoon et al., 1992). Mahdi, syed kazim (2010) examined the seismological characteristics of two double earthquakes (shallow-focused) having M 6.5 that struck the districts of Baluchistan i.e Pishin-Ziarat basin and inferred that the region is extremely vulnerable to seismic risks as it is surrounded through several large thrust and active faults on all sides. These types of earthquakes can occur without forewarning. So, to deal with such calamities and to prevent hazards to become disasters, the public and civil affairs departments must always maintain a common awareness.

Mahdi also discussed about how the thrust and fold belt is not only seismically active but also at risk for future earthquakes, and how the interplay between thrust faults to the east and strike slip faulting to the west may be used to predict seismicity near the province's population centres (Kazim, 2010). The seismic activity and local effects of the site are related to the geological conditions of the area. Seismic activity in Pakistan is characterized by major earthquakes in history and recent times (Ahmad, 2009).

The Sulaiman Range has a high level of seismic activity, according to historical and instrumental evidence and earthquakes with $M_w \geq 6$ rarely occurs. Only three events having $M_w \geq 7$ have occurred in the last century (Ambraseys and Bilham, 2003).

The Sulaiman Range's geodetic data is limited, with no coverage in the range central section. The velocity close to the Chaman fault represents the inter-seismic accumulation of strain nearby the north-south striking left-lateral strike-slip faults and

the motion of Afghanistan relative to India. Further east, in Sulaiman lobe south-west region, estimated velocities indicates that the range interior slides to southeast, towards the Indian Plate interior at ~ 10 to 20 mm per year (Reynolds et al., 2015).

The active faults in the Sulaiman belt are mainly arc-shaped, south convex, thrust/reverse faults following the general structural and topographical features. Photogeological interpretation and teleseismic data are used to locate and identify them. The active faults from north to south are Kakar, Khorasan, Zhob, Mekhtar, Khalifat , Kohlu, Tatra, Harnai and Barkhan faults (Kazmi, 1979a).

Many disasterous earthquakes have been observed in the areas of Baluchistan such as the Quetta earthquake 1935 with Mw 7.4 , the Makran earthquake 1945 with Mw \approx 8.0, Bam, Iran earthquake 2003 with Mw 6.6 , the Mach earthquake 1931 with Mw 7.3 and the recent Ziarat earthquake 2008 with Mw 6.5. Ziarat region have also observed many other earthquakes having M 4.9 in 1893, M 6.1 in 1984, M 6.0 in 1985 and earthquake of M 6.4 in 1997 respectively.

The study is based on the instrumental recorded data and existing fault information (Rafi, 2008).

Because of the active convergence of the Indian and Eurasian plates, seismic activity in Baluchistan is characterized by mid-crustal depth i.e., <50 km. Since there have been many strong earthquakes in the past, their Fault-plane solution shows that the Baluchistan area mainly comprises of left-lateral tectonic regime (Ambraseys and Bilham, 2003).

1.4 Aims of the study

The major goal of our research work is to calculate the stress in the study region and seismic hazard of the same region. Further the findings of our proposed study will be helpful to better prepare the hazard mitigation plans for the vulnerable regions. The objectives of the proposed study are:

1. To compute stresses from static earthquake triggering and produce stress maps of the study area.
2. To outline the seismically vulnerable regions for seismic hazard assessment.

1.5 Methodology

The proposed methodology includes the following steps:

1. The first and most significant phase in seismic hazard analysis is to review the existing literature, which will serve as a source of information for the present work.
2. Then Earthquake catalogue data is required which plays a vital and significant role as it provides a systematic record of recent and historical seismicity.
3. Next step includes earthquake catalogue analysis and data pre-processing which includes data sources and regionwise selection of earthquake events with their associated parameters.
4. Next step includes the stress computation which further includes some model and methods as mentioned in workflow given below (Fig 1.2).
5. Next step includes seismic hazard analysis which includes numerical results and analysis and also the robustness of numerical results.
6. Then we will mark the highly stressed regions leading to vulnerability for hazards.

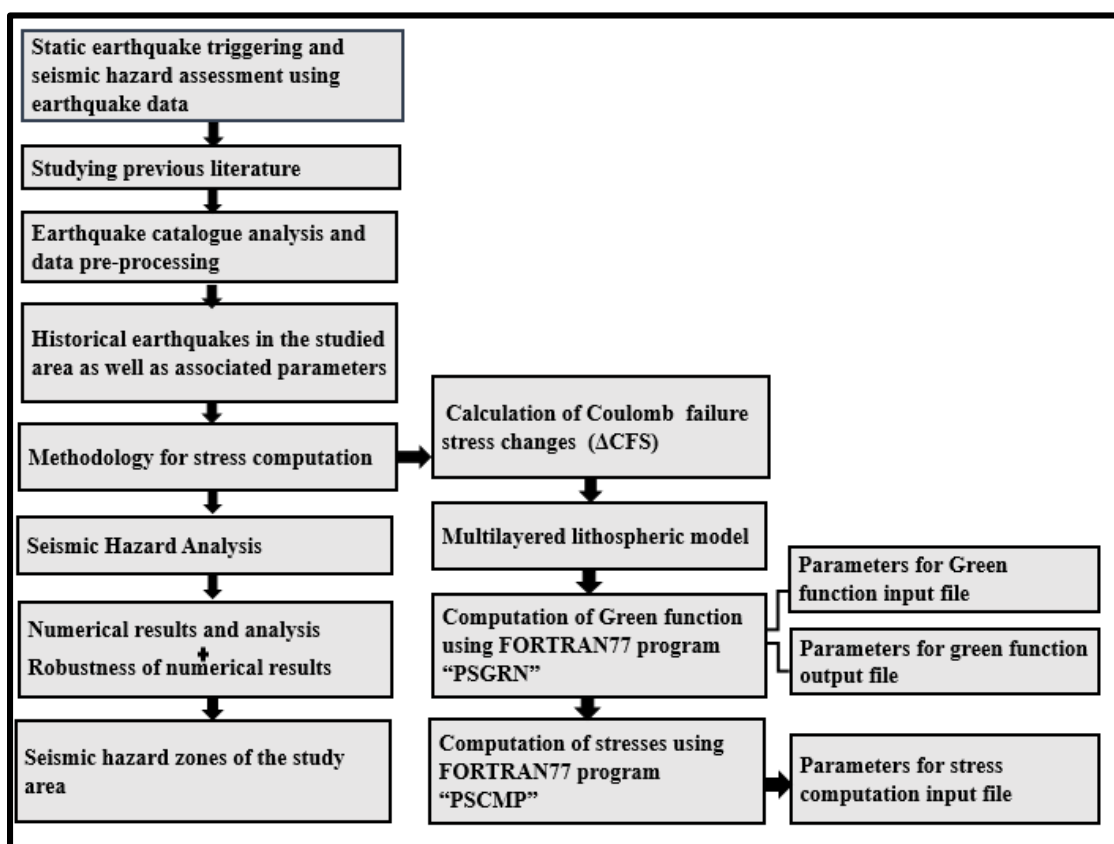


Figure 1.2. Workflow for Seismic Hazard analysis

1.6 Dataset used

Earthquake catalogue data have been taken from USGS, IRIS and old published papers. The following parameters are required for the dataset:

1. Date of occurrence of the earthquake event.
2. Latitude and longitude of the earthquake event.
3. Strike/dip/rake angle of the fault on which the earthquake occurred.
4. Length/width/slip of the earthquake on the causative fault.
5. Magnitude of the earthquake.
6. Focal mechanism solution (FMS) of the earthquake.

PSGRN/PSCMP backend for Pyroko's Green function manager Fomosto : Code to calculate synthetic stress/strain/tilt/gravitational fields on a layered viscoelastic halfspace followed by image plotting using ArcGIS and GMT tools.

CHAPTER 2

TECTONICS AND SEISMICITY OF STUDY AREA

2.1 Regional setting

The regional tectonic environment of Pakistan is revealed via the Eocene Himalayas creation. The Himalayas extends from Burma to the northern Nepal and from India to Pakistan (Gansser, 1981). The Indian plate began to migrate northward after separating from Gondwanaland, eventually colliding with Eurasia. Between the Indian plate (south) and the Eurasian plate (north) is the Tethys Ocean, that is slowly consumed to the continental draft.

The Sulaiman Range is part of the India-Pakistan Plate's northwestern fold-thrust system. The Chaman fault zone borders the Sulaiman fold belt to the west, which is 250 kilometers wide. The tectonic compression between the Indian and Afghan plates generated the foredeep basins in the east and south of the active Sulaiman lobe. Sulaiman lobe was produced by transpression because of left-lateral strike slip motion alongside the Chaman fault and Southward thrusting alongside the Western terminus of the Indian sub-continent (Lawrence et al., 1981; Farah et al., 1984 and Quittmeyer et al., 1979).

2.2 Sedimentary basins of Pakistan

The two main sedimentary basins of Pakistan in terms of origin and different geological histories i.e Indus basin and Baluchistan basin. During the Cretaceous/Palaeocene period, these two basins were formed. The kakar-khorasan Basin, also known as Pishin Basin was recently discovered and developed its own interaction (Raza et al., 1989).

2.3 Indus Basin Geologic history

The Precambrian epoch represents the beginning of geologic time. The Paleotopographic characteristics are extremely important in the formation of the Indus Basin. These characteristics also defined the limit of basin and its division. The ongoing

tectonic and geodynamic processes was further amplified by the configuration of Indus basin. (Raza et al., 1989). Indus basin is further classified into two sub-basins i.e Upper Indus Basin which has further two divisions i.e Kohat-sub basin and Potwar sub-basin and Lower Indus Basin which consists of Central Indus Basin and Southern Indus Basin.

2.4. Central Indus Basin

The research area is located in Central Indus Basin of Pakistan. The Sargodha and Pezu uplifts in the north separate the basin from the upper Indus basin. It is bounded on three sides by the Indian shield in the east, Indian Plate's marginal zone in the west and the Sukkur rift in the south. In fact, Sargodha high is regarded as a dividing line among upper and lower Indus Basin (Kadri, 1995).

The central part of the Indus Basin is divided from east to west into the following broad tectonic divisions (Kadri, 1995).

- a) Punjab Platform.
- b) Sulaiman depression.
- c) Sulaiman Fold and thrust belt.

2.5. Tectonic setting

The main tectonic structures of the Sulaiman region that suggest high levels of seismic activity are complex-shaped of Sulaiman lobe and Sulaiman range, Salt Range, Chaman fault and the Kirthar and Makran range. They form a diffusely deforming zone that adapts to maximum of relative movement between the Indian and Eurasian plates through seismic slip as well as aseismic deformation. The obliquity of the plate margin to the direction of plate convergence shows that complications in the style of deformation is probably the result of strain partitioning (Abdel et al., 1971), an essential phenomenon observed at margins of oblique convergence (Jackson et al., 1995).

The thrust faults and fold axes in both the Salt Range and the Makran Range run east-west, but rotate around the Sulaiman lobe, becoming roughly north-south in the Sulaiman Range. Large strike-slip faults, particularly the Chaman Fault, accompany folds and thrusts and further complicate the structural setting because they strike at an oblique angle to the trends of the folds (DeMets et al., 1994).

The Sulaiman-Kirthar fold belt is 1250 kilometers long and 75-80 kilometers wide. It is a faulted structural zone with thrust belts to the north and west, where the folds of Sulaiman-Kirthar fold belt gradually loses amplitude and merges with the foredeep zone, that is made up of a 10km thick sequence of Jurassic to Recent sedimentary rocks that form massive asymmetrical/upright folds. Based on tectonic style differences and surface features presentation, this fold is divided into the following tectonostratigraphic zones:

1. Sulaiman Arc.
2. Sibi Trough.
3. Kirthar fold belt.

1. Sulaiman Arc

The Sulaiman belt is characterized by east-west running arcuate, convex to the south folds and Jurassic to recent sedimentary rocks are exposed in this belt. The folds are frequently open, parallel/sub-parallel, upright and echelons in this belt. These folds get tighter (asymmetrical) as their topographical relief accentuates northward, exposing older strata in the core of anticlines (Jadoon et al., 1992).

High angle thrust faults such as the Khalifat, Ziarat, Mekhtar, Barkan and Kohlu faults can be found in the northern and central regions of the Sulaiman fold belt. Along eastern as well as western edges of the Sulaiman fold belt, there are numerous significant NW and NNW trending strike-slip faults (Kazmi, 1979a), (Kazmi and Rana, 1982), (Bannert et al., 1992).

2. Sibi Trough

Urak trough, Sibi re-entrant and Sibi depression are all terms used to describe Sibi Trough (Raza et al., 1989a, b). Sibi trough is bordered on the east and west through the Sulaiman arc and Kirthar fold belt, and on the north and south through the Zhob thrust-belt and Kirthar foredeep respectively.

3. Kirthar Fold Belt

Between Quetta and Karachi, this belt forms a 50-70km broad and ~380km long, north-south trending folded zone. The Bela-Zhob ophiolite and thrust belt surround it to the north and west, while the Sibi Trough, Kirthar foredeep and Indus platform surround it to the east.

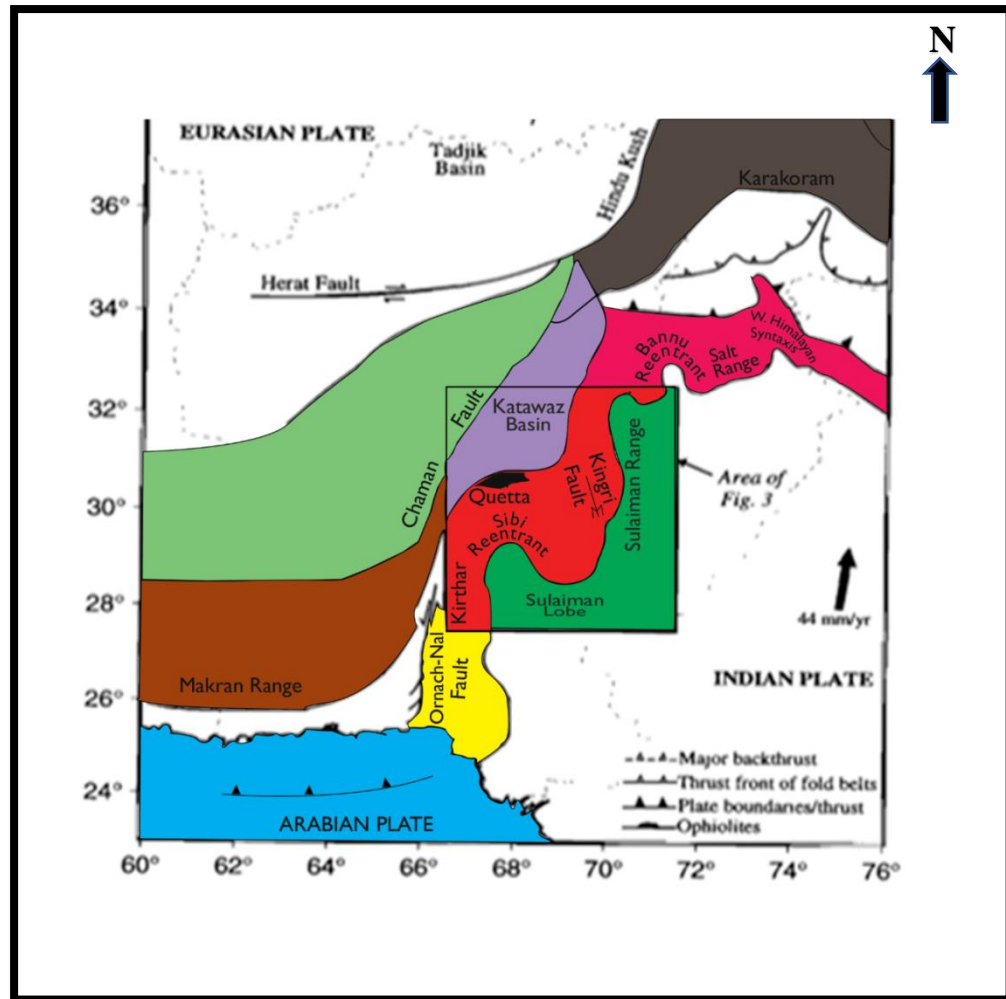


Figure 2.5. Geographic and tectonic setting of the Sulaiman lobe and Range (Jadoon et al., 1994; Banks & Warburton, 1986)

2.6. Geological setting

The Sulaiman fold and thrust belt which includes the Sulaiman Range in the east, the interior Loralai Range and the Southern Mari-Bugti Hills is the world's largest fold-thrust belt. It is made from Mesozoic platform carbonates, muds, sands, shales and volcanics, all of which indicates deep water proximity to the north. These deposits migrated northward from the newly shaped Himalayas to Eocene sandstones, mudstones, shales and volcanic rocks with proximity to deep water. From the Eocene onwards, these deposits have been transformed into newer siliclastic sediments shed from newly formed Himalayas, deposited in a shallow deltaic environment. (Qayyum et al., 2001).

In the early Cenozoic, sedimentary strata was formed in a huge basin in the western Indo-Pakistan subcontinent and eventually the Neo-Tethys Ocean developed

northward. The Katawaz Basin sequence, which is located directly east of the Chaman fault, was named after it (Qayyum et al., 1996). The equal time-transgressive clastic succession extends into the Sulaiman foredeep and is covered with younger Himalayan molasses. The Sulaiman Range is the elevated and deformed passive margin sequence of the Indian Plate northwestern boundary, which has bow accreted to the Afghan Block's eastern edge and is being underthrust by the Indian Plate.

2.7. Stratigraphic sequence of Sulaiman Lobe

In study area, Permian to Recent clastics and carbonate sediments are present, and probably the Cambrian succession is similar to the one that occurs in the Kohat-Potwar Fold Belt. In southeast, the succession is younger as compared to northwest direction. In Permian and Jurassic, there is distinct break in the intraformational sediments, while there is regional unconformity in Cretaceous and Tertiary strata. Jurassic rocks are exposed in some parts of the basin because of intense erosion.

2.8. Seismicity of study area

Pakistan has large areas of moderate-to-high seismicity, with a number of seismic tectonic features caused by a network of interconnected active faults. The following are the most important seismic zones in the research area:

The entire Sulaiman fold-and-thrust belt, which is characterized by shallow earthquakes of moderate to high magnitude i.e 5 to 7, is included in the Sulaiman seismic zone. The Harnai-Kohlu seismicity belt, which is arcuate and 20-25 km broad, is located inside this zone. A succession of major North-east, East-west and North-west trending faults run across the Harnai-Kohlu high seismicity area (Quittmeyer et al., 1979).

According to the Focal mechanism solutions related with the earthquakes occurred in the Harnai-Kohlu belt indicates that strike-slip faulting and thrust faulting dominates in this region as shown in Fig 2.1. The seismicity in the other areas of the Sulaiman range is more diffused as seen by the vast spread of seismic events (Molnar et al., 1973), (Chandra, 1978).

The Kacchi plain to the east and the Ghazaband fault to the west, which separates the Kirthar-fold-and-thrust-belt from the Chaman fault seismic zone, limit the northern portion of this belt between Quetta and Kalat. As evidenced by seismic occurrences and

associated ground ruptures at various areas, the seismicity of this region is centered around a few N-S trending faults, particularly the Quetta, Ghazaband, Johan, Chiltan, Nagau and Mach faults (Armbruster et al., 1980).

The Chaman fault seismic zone forms a narrow seismic strip around the 900-kilometer-long Chaman fault and contains moderate-to large- earthquakes, with smaller earthquakes occurring more recently. The southern extrusion of the Sulaiman Lobe is accommodated by the left-lateral Kingri fault that runs along the eastern margin of the lobe (Rowlands et al., 1978). The main thrust faults in the region includes Pirkoh thrust, Karmari thrust, Karahi thrust, Chinjan thrust and Zhob valley thrust (Bender and Raza, 1995).

In Ghazaband Pass Kirdap region, the Ghazaband fault is a NNE-SSW orientation fault. The fault is partially concealed under alluvium. It merges with the Chaman transform fault system as it moves southward.

A local NNW-SSW dextral shearing alongside the western boundary of the Sulaiman lobe accommodates its southward movement in relation to the Kirthar range and its westward movement in relation to the Afghan block accommodating their distinct shortening rates.

The Urghargai fault, a 150km long right-lateral strike slip fault accommodates this relative motion (Kazmi, 1979). The Quetta Syntaxis, located at the intersection of the Kirthar range and southwestern encroaching Sulaiman Lobe, is the most seismically active area of the western Indian Plate margin. In the south-east direction, seismicity becomes more diffuse and thrust fault mechanism become more dominant (Bernard et al., 2000).

At least four earthquakes with $M_w > 6$ have impacted this seismic region in the last century. These earthquake includes:

- a) The 1931 Sharigh earthquake with M 6.8 (Ambraseys & Bilham, 2003).
- b) The 1997 Harnai earthquake (Bernard et al., 2000).
- c) The two Ziarat events in 2008 (Yadav et al., 2012).

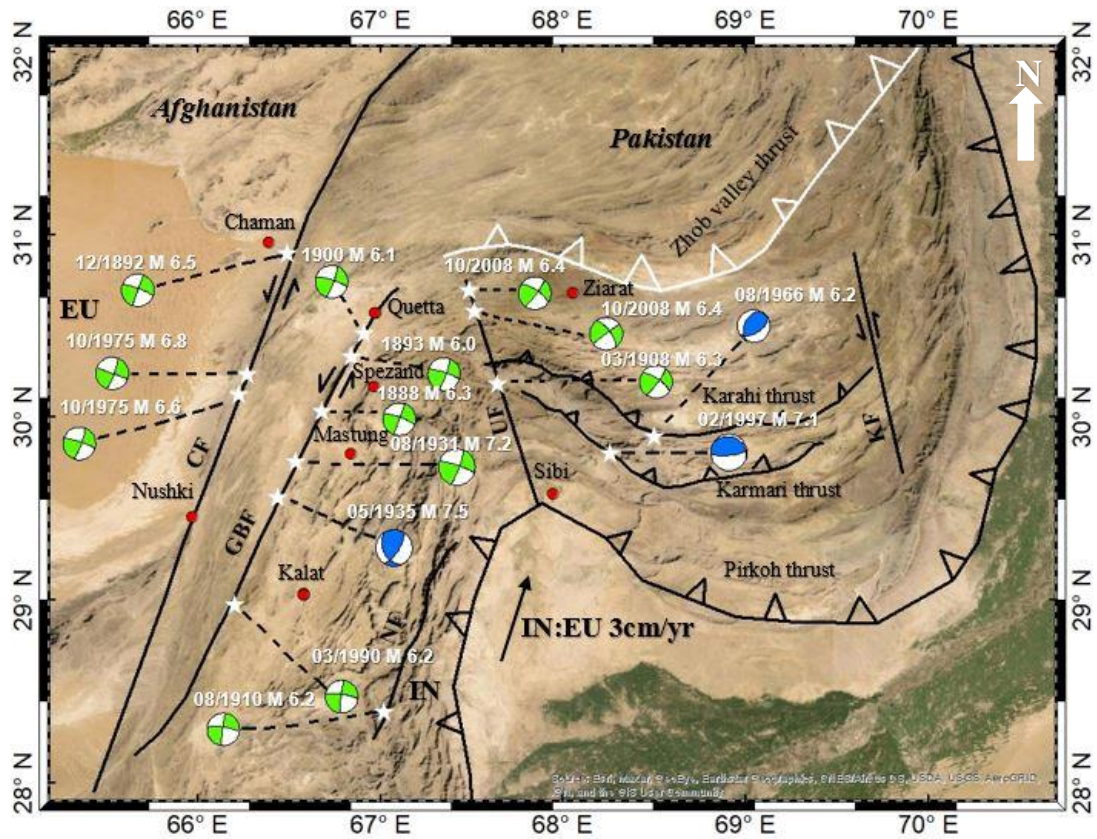


Figure 2.1 Seismotectonic map of study area. The white star represent the earthquakes with their related focal mechanisms, selected for our study for the period 1888-2008. The Red circle represent major cities in the study region. Heavy black lines represent the major faults and thrusts in the study area. CF Chaman Fault, GBF Ghazaband Fault, NF Nagau Fault, UF Urghargai Fault, KF Kingri Fault, Karahi thrust, Karmari thrust, Zhob Valley Thrust, Pirkoh Thrust, IN Indian Plate, EU Eurasian Plate.

CHAPTER 3

EARTHQUAKE CATALOGUE ANALYSIS AND DATA PRE-PROCESSING

3.1. Introduction

The main sources of the information for the present hazard evaluation are the Earthquake catalogues. A robust earthquake catalogue is required for reliable seismic hazard evaluations. The longer the extent of the catalogue, the more reliable the parameters and more useful it is for assessing the risk of earthquakes (IAEA, 2008).

3.2. Data sources

Data from earthquake catalogues is crucial since it gives a systematic record of recent and past seismicity. Data for the earthquake catalogue was gathered from a variety of sources including previous published papers and from the catalogues which had been already developed by different national and international agencies such as PMD, USGS, ISC etc. The main catalogues which have been used as basis for the present study includes:

1. Pakistan Metrological Department (PMD) historical Database.
2. United States Geological Survey (USGS), National Earthquake Information Center (NEIC).
3. CMT catalogue (Harvard Centroid Moment Tensor Project, 2009).
4. ISC, International Seismological Centre England, database.

In this study, keeping in view the objectives of this study, a refined earthquake catalogue is prepared by manipulating the above-mentioned catalogues for the study area.

We rigorously inspected both published and online earthquake databases (Ambraseys and Bilham, 2003). A new catalogue file of the study region with the help

of above-mentioned data sources is compiled. The primary compiled catalogue is comprised of 72 earthquakes having magnitudes (M_w) ranging from 5.5 to 7.5. Out of these 72 earthquakes, The final catalogue file is prepared which include 15 earthquakes with Magnitude (M_w) ranging from (6.0-7.5). We chose only those earthquakes with magnitude ranging from 6.0-7.5 as the CFS impact of earthquakes with $M < 6.0$ is not much significant. The final catalogue consists of following parameters:

1. Date of occurrence of the earthquake.
2. Latitude and longitude of the earthquake.
3. Magnitude of the earthquake.
4. Focal mechanism solution (FMS) of each earthquake.
5. Rupture length, rupture width and fault slip caused on the causative fault by the respective earthquake.

3.3 Earthquake Parameters Calculation using empirical relation

The moment magnitude, surface rupture length, subsurface rupture length, downdip rupture width, rupture area, and maximum and average displacement per event are all compiled from historical earthquake parameters from around the world. (Coppersmith et al., 1994).

If the magnitude of the earthquake event is known, then we can calculate the length of the rupture, rupture width and average slip of that particular earthquake using the scaling relation and vice versa. With the help of the equations (Coppersmith et al., 1994), reported in table 3.1, for strike slip, reverse and normal faults, we calculated the rupture width, rupture length and average slip for all the selected earthquakes in the final catalogue.

Table 3.1. Earthquake parameters using empirical relation

Empirical relation source parameters	Equation	Slip Type	Co-efficients and standard errors	
			a	b
Rupture length	$\log(\text{SRL}) = a + b * M$	Strike-slip (SS)	-3.55	0.74
		Reverse (R)	-2.86	0.63
Rupture width	$\log(\text{RW}) = a + b * M$	Strike-slip (SS)	-0.76	0.27
		Reverse (R)	-1.61	0.41
Average slip	$\log(\text{AD}) = a + b * M$	Strike-slip (SS)	-6.32	0.90
		Reverse (R)	-0.74	0.08

From the table 3.1, using the empirical relation we calculated the source parameters i.e., rupture length, rupture width and average slip (as mentioned below) of the respective earthquakes for the final catalogue. The final catalog with all necessary information, obtained/ calculated, is stated in table 3.2.

Table 3.2. Historical earthquakes in the studied area, as well as associated source parameters.

Sr. No	DD-MM-YYYY	Magnitu-de (Mw)	Earthquake epicenter Lat/long	Strike/dip/rake	Length/width/slip (km/km/m)
1	28-10-1888	6.3	30.03842/ 66.68609	20/90/10	12.9/8.7/0.22
2	20-12-1892	6.5	30.89788/ 66.49823	20/90/10	18.2/9.9/0.34
3	13-02-1893	6	30.33823/ 66.8479	20/80/9	7.8/7.2/0.12
4	00-00-1900	6.1	30.46303/ 66.91464	20/80/9	9.2/7.7/0.15
5	05-03-1908	6.36	30.1888/ 67.64513	304/73/171	14.3/9.1/0.25
6	17-08-1910	6.26	28.38722/ 67.01847	278/78/-176	12.1/8.5/0.21
7	27-08-1931	7.24	29.76347/ 66.54344	20/80/9	64.2/15.7/1.57
8	30-05-1935	7.4	29.56538/ 66.44589	33/68/124	84.3/17.3/2.19
9	01-08-1966	6.2	29.89847/ 68.50742	204.8/42.7/62.6	11.1/8.2/0.57
10	03-10-1975	6.8	30.24115/ 66.27456	20/80/0.34	30.3/11.9/0.63
11	03-10-1975	6.6	30.12693/ 66.23173	20/80/10	21.6/10.5/0.42
12	04-03-1990	6.2	28.97825/ 66.21032	278/78/-176	10.9/8.2/0.18
13	27-02-1997	7.1	29.80805/ 68.26472	85/77/82	50.6/14.4/1.17
14	28-10-2008	6.4	30.698/ 67.49285	304/73/171	15.3/9.3/0.28
15	29-10-2008	6.4	30.58379/ 67.5214	324/68/-178	15.3/9.3/0.28

The required details of all the earthquakes and the faults on which these earthquakes occurred are reported in the catalogue (table 3.2), and are described below in the following section along with their location map.

3.3.1. The 1888 Quetta Earthquake (M=6.3)

On September 28, 1888, a M 6.3 magnitude earthquake struck the Quetta, destroyed the city. The earthquake epicenter was at 30.03°N and 66.6°E respectively. This earthquake was recorded as having a maximum intensity of VIII-IX. The 1888 earthquake was occurred on the Ghazaband fault (Zahid, 2014).

3.3.2. The 1892 Chaman Earthquake (M=6.5)

The 1892 earthquake was occurred in the region of Chaman, some ~90 km north to Quetta, near Pakistan-Afghanistan border. It resulted in significant deformation of the recently constructed train track that crossed the Chaman fault, depicted a transform faulting style. The minimal rupture length, the very small area over which the earthquake was felt and early teleseismic instrumentation data all point to a surface wave magnitude M_s 6.8. The earthquake epicenter was at 30.89°N and 66.49°E respectively. Shelabagh railway station building was severely destroyed by the 1892 earthquake (Griesbach, 1893).

3.3.3. The 1893 Quetta Earthquake (M=6.0)

The 1893 earthquake with Magnitude of 6.0 struck in Quetta city on February 13, 1893. The epicenter of the earthquake was at 30.33°N and 66.84°E. Although the earthquake prompted some alarm in Chaman, no damage was observed. This earthquake at Quetta was substantially greater than the one that struck 1892 earthquake. The Ghazaband fault appears to be the source of this seismic activity and the FMS implies a left-lateral faulting trend (Ambraseys and Bilham, 2003).

3.3.4. The 1900 Quetta-Pishin Earthquake (M=6.1)

Quetta-Pishin earthquake with M 6.1, impacted Quetta-Pishin district, with the epicenter at 30.46°N and 66.91°E respectively. The causative fault of this earthquake was Ghazaband fault. This earthquake's fault-plane solution reveals a left-lateral trend (Zahid, 2014).

3.3.5. The 1908 Earthquake (M=6.3)

On March 5, 1908, an earthquake with M 6.3 struck near Urghargai and Ziarat district in Baluchistan. Urghargai fault appears to be the source of this seismic activity. The epicenter of this earthquake was around 30.1°N and 67.6°E. The fault-plane solution in the area reveals a right-lateral trend (Zahid, 2014).

3.3.6. The 1910 Ghazaband Earthquake (M=6.2)

The 1910 earthquake with Mw 6.2 occurred on August 17, 1910 near Nagau, a mountain range located in the Kalat district of Baluchistan. The epicenter of this earthquake was at 28.3°N and 67.01°E respectively. Nagau fault seems to be the cause of this seismic activity.

3.3.7. Mach Earthquake 1931 (M=7.2)

The 1931 earthquake occurred on 27 August 1931 with M 7.3 (Ambraseys and Bilham, 2003) and was felt in Baluchistan and Sindh with a reported depth of 33km. 120 deaths were reported due to Mach 1931 earthquake (Szeliga).

3.3.8. The Quetta Earthquake 1935 (M=7.4)

On May 30, 1935, a M 7.7 magnitude earthquake struck Quetta, the Capital of Baluchistan province. It was reported as very shallow earthquake with a depth of 10 km. This renowned earthquake claimed the most lives than any other earthquake in the Indian subcontinent at that time. The Ms of the Quetta earthquake was assessed to be 7.7. The causative fault of 1935 earthquake was the Ghazaband fault.

According to the 1978 temporary seismic network, Microseismicity was concentrated towards the rupture's end sites (Armbruster et al., 1980). The deaths reported as a result of this earthquake was around 35,000, although the total count is still unknown.

3.3.9. The 1966 Duki Earthquake (M=6.2)

The 1966 earthquake M 6.2 occurred on August 1, 1966 near Duki, district in the Baluchistan province of Pakistan. The epicenter of this earthquake was at 29.8°N and 68.5°E respectively. This earthquake occurred on the thrust fault named as Karahi thrust (Bender and Raza, 1995).

3.3.10. The 1975 Chaman Earthquake (M=6.8 and M=6.6)

In 1975, an earthquake with M 6.8 struck the Chaman fault zone near the Afghan border in Spin Tezha, followed by another event with a Mw 6.6, ~12 hours later by the 1st event. Except for some minor damage in Quetta, little is known about the effects of these events in the epicentral region of the Afghan border, which is thinly populated. These tremors were felt most intensely in Quetta and northwestern Baluchistan.

About 5 kilometers south of Spin Tezha, near the Chaman fault zone, a trace of north-south trending discontinuous surface fault rupture was observed in alluvium, which was probably only a minor segment. It exhibited a 4cm average left-lateral displacement with slight dip-slip up to the west, which was consistent with the focal mechanism of the earthquake (Farah et al., 1976).

3.3.11. The 1990 Earthquake (M=6.2)

The 1990 earthquake with Mw 6.2 struck the city of Quetta on March 04, 1990. The epicenter of this earthquake event was at 28.97°N and 66.21°E respectively. Ghazaband fault was the possible source of this earthquake. The focal mechanism solution indicates left-lateral faulting trend.

3.3.12. Baluchistan Earthquake February 27,1997 (M=7.1)

A powerful earthquake occurred in the central region of Pakistan on 27th February 1997. This earthquake was located in the seismotectonic province of Kirthar-Sulaiman shear zone, near the town of Harnai which is about 60km ENE of Sibi and 100km SE of Quetta. The body wave magnitude of the main shock on the Richter scale was 6.2 and it was located at 29.98°N, 68.22°E with depth of less than 10km.

3.3.13. Ziarat (Baluchistan) Doublet Earthquakes 2008 (M= 6.4)

The 2008 devastating doublet earthquakes of M 6.4 occurred in the Chiltan hills which destroyed a large area of the province of Baluchistan. It occurred to south-west of Pakistan on October 28th, 2008 at 23:09:57 GMT. The 1st event of this doublet was occurred at a distance ~51.4km NW ziarat and about 60km NE Quetta. The epicenter of 1st event was at latitude 30.53°N and longitude 67.53°E. Another earthquake of same magnitude, M6.4, occurred 12 hours after the 1st event, and it was occurred ~25km SE of the 1st event. Due to their identical magnitudes (6.4), similar focal mechanism solutions and focal depth, these earthquakes were named as Ziarat Doublet earthquakes (ZDE). This doublet earthquake is the strongest and deadliest in Baluchistan region since Harnai 1997 earthquake which caused widespread destruction in the region as discussed above. The epicenter of this seismic activity lies in the structurally complex Sulaiman-Kirthar fold and thrust belt which is 1250km long and 75-180km wide and it lies between Pishin, Muslim bagh and Ziarat area. The epicentral location of Ziarat doublet earthquake is situated on the Urghargai fault. The focal mechanism solution of the fault planes i.e strike NNW-SSE dips 79° and 78° NNE and 10km depth of FMS

are the indicative of the activation of this NNW-SSE 10-15km deep fault whereas the patterns of the aftershocks also supports the view that the Urghargai fault is the causative fault of 2008 Ziarat Doublet Earthquake (Jan, 2010).

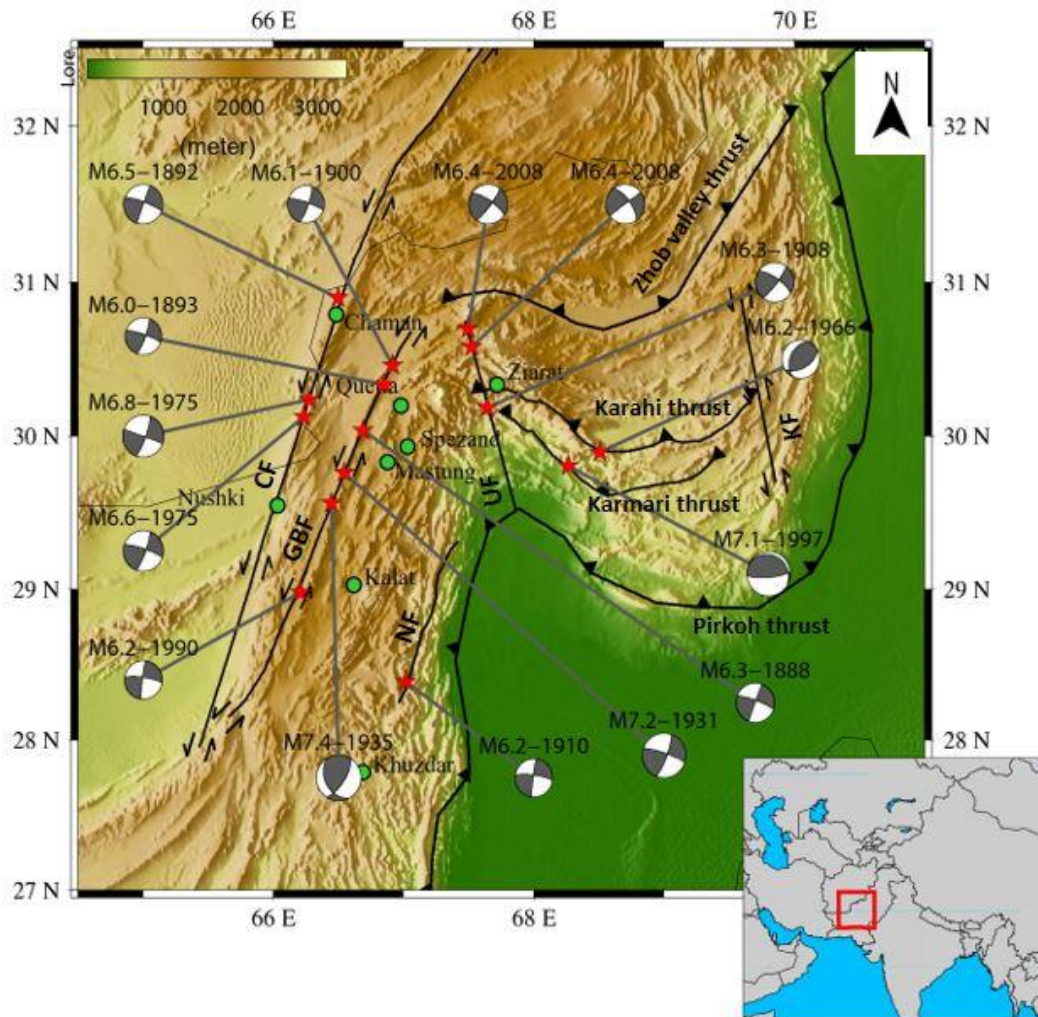


Figure 3.1 Location map of all 15 selected earthquakes. Green circles indicates the major counties in the study area. The red star shows the focal mechanism solution of all the earthquakes. Heavy black lines represent the major faults and thrusts in the study area. CF Chaman Fault, GBF Ghazaband Fault, NF Nagau Fault, UF Urghargai Fault, KF Kingri Fault, Karahi thrust, Karmari thrust, Zhob Valley Thrust, Pirkoh Thrust.

CHAPTER 4

METHODOLOGY FOR STRESS COMPUTATION

4.1 Introduction

“Stress transfer” refers to the process by which a stress perturbation is communicated to the fault. As the sources of stress changes and processes of stress transfer vary temporally and spatially, hazard assessments also must account for these variations. Understanding and quantifying this is the realm of “time-dependent seismic hazard. The three primary sources of stress transfer includes tectonic loading, static earthquake stress transfer and viscoelastic stress transfer. In this study static earthquake stress transfer and viscoelastic stress transfer will be incorporated while tectonic loading will remain fixed.

4.2. Model and methods

The model and methods for stress computation have been explained in the following sections.

4.2.1 Calculation of Coulomb Stress Changes

Our research was carried out by determining the change in Coulomb failure stress owing to earthquake using the following expression (Scholz, 1990).

$$\Delta CFS = \Delta \tau + \mu' \Delta \sigma N \rightarrow (i)$$

Where, τ =shear stress, σ = normal stress, μ' = effective co-efficient of friction.

The change in normal shear stress represents the slip direction for a subsequent event (the receiver), where $\Delta \sigma N$ is positive for rising clamping normal stress with pressure specified positive. Regional faults which are closer to failure lies in positive ΔCFS zones, whereas faults which are further away from the failure lies in negative ΔCFS zones according to the equation (i) (Freed, 2005).

The focal mechanism solution for the earthquakes that were chosen, as well as the receiver fault parameters employed in this current study, are stated in Table 3.2. For

the determination of co-seismic and post-seismic stresses, we employed a model with dislocation sources enclosed in a layered half space with mixed elastic and inelastic properties. We also employed the PSGRN/PSCMP programmes (Wang et al., 2006) which allow us to calculate surface and subsurface deformation caused by geophysical sources in a multilayered viscoelastic gravitational half-space. Finally, since the 1888 earthquake, we computed the CFS on the receiver fault using both co-seismic static and viscoelastic stress transfer changes.

We chose linear Maxwell rheology over a complicated rheological model to calculate the viscoelastic effect in this study because viscoelastic relaxation at a temporal scale of 100 years indicates negligible differences in stress changes (Verdechia and Carena, 2015). Due to the scarcity of geodetic measurements in the studied region, we used a moderate value of 1×10^{19} Pa s for viscosities of both lower crust and upper mantle performed simulation at 10km depth. The robustness of numerical results will be investigated further by choosing different values of viscosity for the lower crust and upper mantle. (Discussed in Chapter 5).

4.2.2. Multilayered Lithospheric Model

A 1D layered structural model (stair-case model) has been utilized for the computation of green function, reported in table 4.1. We created a reference lithospheric model consisting of upper, middle and lower crust as well as lithospheric mantle based on crust 1.0 (<https://igppweb.ucsd.edu/~gabi/crust1.html>) due to non-availability of both local seismic observations and different velocity patterns of the region of interest. There will be fewer than 40 crustal types included in CRUST 1.0. Each of the 1x1-degree cells will have its own 8-layer crustal profile consisting of : 1) water ,2) ice, 3) upper sediments, 4) middle sediments, 5) lower sediments, 6) upper crust, 7) middle crust and 8) lower crust.

Seismic studies determine the thickness, density, V_p and V_s of each layer. The shear modulus is calculated using the formula (eq ii) (Aki and Richards, 2002).

$$\mu = \rho V_s^2 \approx 1/3 \rho V_p^2 \rightarrow (ii)$$

We selected a moderate value of 0.4 for the co-efficient of friction (μ') in our simulation (King et al., 1994). Based on the structure (1D velocity model) of our study area for which we want to calculate the stresses, and to analyze to the response of the stresses that how it will behave, computation of green function is necessary. We employed two programs/utilities for the computation of stresses i.e PSGRN and PSCMP codes (Wang et al., 2006), to achieve the objective of this study. PSGRN is employed to compute the Green function of the region being studied, followed by the calculation of co-seismic and post-seismic stress by employing PSCMP.

Table 4.1. Parameters of 1D multilayered model

Depth (km)	Vp (km/sec)	Density (kg/m ³)		
0-20	6	2720	Upper Crust	Elastic
20-30	6.3	2790	Lower Crust	Viscoelastic
30-40	6.5	2850		
40-100	8.2	3340	Upper Mantle	

4.3. Computation of Green function using FORTRAN77 program “PSGRN”

The Green's function is defined empirically as the impulse response of the medium. With regard to a signal being received by sensors at two different locations, the Green's function translates to Earth's response between two receivers. Based on the structure (1D velocity model) of our study area for which we want to calculate the stresses, and to analyze the response of the stresses that how it will behave, computation of green function is necessary.

For the computation of green function, we will have to set the input file that comprised of multiple parameters, which are used for the calculation of green function.

The input file for the FORTRAN77 software 'PSGRN' which is used to compute the responses (Green's function) of a multilayered viscoelastic half-space to point dislocation sources buried at various depths. For our studies, we chose the 10km as seismogenic depth. PSGRN software is also used for the calculation of time-dependent viscoelastic relaxation.

4.3.1 Parameters for Green function Input file

Table 4.2. Parameters for Green function Input file

No	Parameters	Description
1	Source-observation configurations	<p>a. The first parameter for source-observation configurations includes the depth and the type of earthquake.</p> <p>The point on which observation will be taken, what will be its depth because on a particular depth, Green function response will be generated. Normally, Green function is generated at 10km depth because it is a seismogenic depth but if we want to plot the cross-section, then the depth can be selected at 5km, 10km or 15km etc for the computation of green function depending on the objectives.</p> <p>Next, we must have to choose between oceanic (0) or continental (1) earthquakes for the uniform depth of the observation points (km).</p> <p>We selected 10km depth of the observation points and switched for continental (1) earthquakes for the computation of green function.</p> <p>b. Second step includes:</p> <ul style="list-style-type: none"> • Number of observations. • Start and end distance and the interval between them. <p>Less interval leads to increase in resolution due to which computational time also increases and vice versa.</p>

		c. Third is the number of equidistant source depth.
2	Time-sampling	It includes: a. Number of time samples and time-window. For how many number of days, green function is calculated.
3	1-D velocity model	It includes depth, V_p , V_s , Rho , as well as lower crust and upper mantle viscosities.

4.3.2. Parameters for Output file

Table 4.3. Parameters for green function output file

No	Parameters	Description
1.	Output directory	After the calculation of the Green function, it needs to be stored in output directory. We have to give the path to the output directory with the file name.
2.	3 Displacement components file names	U_z , u_r and u_t are the three displacement components that will be determined.
3.	6 Stress components file names	The 6 stress components which will be calculated i.e. s_{zz} , s_{rr} , s_{tt} , s_{zr} , s_{rt} , s_{tz}

4.4. Computation of Stresses using FOTRAN77 “PSCMP”

After the calculation of green function using program ‘PSGRN’, ‘PSCMP’ program is employed for the co-seismic and post-seismic stresses calculation based on Green function, already computed employing the ‘PSGRN’ program. An arbitrary number of rectangular dislocation planes depicts the earthquake source.

After the calculation of green function, we have to compute the CFS caused by the respective earthquake on the receiver fault as well as on the nearby faults of the region.

4.4.1. Parameters for Stresses computation input file

Table 4.4. Parameters for Stress computation input file

No	Parameters	Description
1	Observation array	<p>The first parameter includes which type of observation will be selected.</p> <p>Observation array can be selected by three ways:</p> <ol style="list-style-type: none"> a. Irregular observation position, for this observation position we have to select (=0). b. 1D observation profile, in this profile starting and ending latitude longitude positions are given after which it plot the lines automatically. For this profile we have to select (=1) c. Rectangular 2D observation array, in this array , the latitude and longitude positions of every given point is required. For this we have to select (=2)
2	Orientation of receiver faults	<p>Second parameter includes the orientation of the receiver fault:</p> <ol style="list-style-type: none"> a. Selection of (1/0) for los displacements (only for snapshots). It will remain fixed. b. For coulomb stress changes, select (1/0) output (only for snapshots): The consistent regional master fault mechanism is described by icmb, friction (which varies from 0.2-0.8), Skempton ratio, strike, dip and rake angles. In arbitrary order, the uniform regional principle stresses i.e sigma1, sigma 2 and sigma 3 (Pa) triggering value-(0.0.1 Mpa). Assuming that the master fault is oriented optimally according to the Coulomb failure stress criterion, the orientation of the pre-stress field will be calculated.

		<p>The following information will be included in the snapshots if this option is set i.e icmb=1.</p> <p>On the master fault, CMB_Fix, Sig_Fix= Coulomb and normal stress changes.</p> <p>Str_Op1/2, Dip_Op1/2, Slp_Op1/2=strike, dip and rake angles of the two optimally oriented faults.</p> <p>c. Output directory in char format i.e outdir</p> <p>d. Outputs for displacement components selection (1/0=(yes/no)</p> <p>e. Selection of file name for the x,y and z components.</p> <p>f. Outputs for stress components selection (1/0=yes/no)</p> <p>g. Choosing a file name for all the six stress components i.e xx,yy,zz,xy,yz and zx respectively.</p>
3	Green's Function Database	<p>a. A directory containing green function. We have to give the path of the green function here.</p> <p>b. File names for the Green's function:</p> <p>3 displacement components</p> <p>4 stress components</p>

```

# RECTANGULAR SUBFAULTS
# =====
# 1. number of subfaults (<= NSMAX in pscglob.h): ns
#
# 2. parameters for the 1. rectangular subfault: geographic coordinates
#    (0_lat, 0_lon) [deg] and 0_depth [km] of the local reference point on
#    the present fault plane, length (along strike) [km] and width (along down
#    dip) [km], strike [deg], dip [deg], number of equi-size fault patches along
#    the strike (np_st) and along the dip (np_di) (total number of fault patches
#    = np_st x np_di), and the start time of the rupture; the following data
#    lines describe the slip distribution on the present sub-fault:
#
#    pos_s[km] pos_d[km] slp_strike[m] slp_downdip[m] opening[m]
#
#    where (pos_s,pos_d) defines the position of the center of each patch in
#    the local coordinate system with the origin at the reference point:
#    pos_s = distance along the length (positive in the strike direction)
#    pos_d = distance along the width (positive in the down-dip direction)
#
# =====
# n_faults
# -----
#
# 1
# -----
# n  0_lat  0_lon  0_depth length width strike dip  np_st np_di start_time
# [-] [deg]  [deg]  [km]   [km]  [km] [deg] [deg] [-]  [-]  [day]
#    pos_s  pos_d  slp_stk slp_ddip open
#    [km]   [km]   [m]     [m]     [m]
# -----
# 1  30.2  67.00   10.0  42.7   13.5   20  90  1  1  0.0
#    0.0   0.00   0.95  0.0   0.000
# =====end of input=====

```

Figure 4.1 Input file parameters (Stresses computation)

CHAPTER 5

RESULTS AND DISCUSSION

We computed the co-seismic and post-seismic stress changes caused by the earthquake sequence, oldest occurred in 1888 and latest occurred in 2008 using elastic dislocation theory and a multi-layered lithospheric model. We also examined the relationship between these events as well as the influence of one earthquake on the impending earthquakes.

The lower crust and upper mantle are assumed to be fully elastic for the computation of both co- and post-seismic stress. The co-seismic and post-seismic changes caused by the 1888-2008 earthquake sequence have been described below with the figures. Our main results are deduced by using moderate values of viscosities ($1 \times 10^{19} \text{ Pa s}$) for both lower crust and upper mantle to estimate the seismic hazard assessment.

5.1. Numerical results and Analysis

5.1.1. Co-and Post-seismic stress changes (Mw 6.3 1888 Earthquake)

The Mw 6.3 Ghazaband earthquake occurred on September 28, 1888 and the epicentral location (30.03842°N , 66.68609°E) of this earthquake is situated on the northern segment of the Ghazaband fault. According to the scaling law (Table 3.1), computed results are stated in table 3.2, the rupture length, rupture width, and uniform slip of 1888 earthquake is 12.9km, 8.7km and 0.22m respectively. We computed the co-seismic coulomb stress changes caused by 1888 Ghazaband earthquake using stress triggering theory and a multilayered lithospheric model, snapshot reported in Fig 5.1. From the fault plane solution of the Mw 6.3 1888 event, the receiver fault parameters are taken as strike= 90° , dip= 20° and rake angle= 10° .

Figure 5.1(a) reports the co-seismic CFS changes at $\sim 10\text{km}$ depth with an effective co-efficient of friction of 0.4 caused by this earthquake. The significant features are the presence of lobes created by the stress release/transfer by the 1888

earthquake. The warm red lobes indicate the regions with enhanced Coulomb stress as a result of co-seismic displacement on the faults which raises the coulomb stress in some areas and may induce seismic activity. The blue lobes indicating the stress, the region which has released the stress on faults, and eventually may depress the forthcoming seismic activity.

Figure 5.1(a) shows that the co-seismic static stress transfer caused by the 1888 Ghazaband earthquake leads the CFS increment on the North-east as well as south-western part and CFS decrement on the NNW-SSE part. The maximum and minimum Δ CFS changes caused by 1888 Ghazaband earthquake event are 0.2607MPa and -3.42MPa respectively. The snapshot of post-seismic stresses caused by the 1888 earthquake's viscoelastic relaxation is reported in Fig 5.2(a). The significant contribution of viscoelastic stress transfer is manifested in the snapshot, where the size of the lobes has increased.

5.1.2 Co-and Post-seismic stress changes (Mw 6.5 1892 Earthquake)

The magnitude 6.5 Chaman earthquake, occurred on 20 December, 1892 with the epicenter located (30.89788°N, 66.49823°E) on the northern segment of the Chaman fault. According to the scaling law (Table 3.1), computed results are stated in table 3.2, the rupture length, rupture width and uniform slip of 1892 Chaman earthquake is 18.2km, 9.9km and 0.34m respectively.

Figure 5.1(b) reports the co-seismic CFS at ~10km depth with an effective coefficient of friction i.e 0.4. From the focal mechanism solution of the Mw 6.5 1892 event, the receiver fault parameters are taken as strike=90°, dip= 20° and rake angle=10. This earthquake is purely a strike-slip event. Co-seismic coulomb stress changes associated with 1892 Chaman earthquake shows that this event has generated positive stress on the north-south and east-western lobes indicating highly stressed regions and negative stress on NNW and SE lobes indicating stress shadow zones respectively (Fig 5.1b).

Since there is a 04 year interval between 1888 Ghazaband and 1892 Chaman earthquake, Maxwell body model has been used to simulate post-seismic viscoelastic relaxation and quantify the impact of 1888 Ghazaband earthquake on the 1892 Chaman earthquake. (Fig 5.2a). The stress field state is then presented for a period of time just before each subsequent event. The Δ CFS immediately before the 1892 earthquake is

shown in fig.5.2b which is indicating the position of the stresses associated with the 1888 Ghazaband earthquake with the occurrence of the subsequent event. Figure 5.2b indicates that 1892 earthquake is an independent earthquake. There is negligible interaction between these two events which indicates that it has not been triggered by the preceding earthquake. The maximum and minimum Δ CFS changes caused by 1892 Chaman earthquake event are 2.7MPa and -3.92MPa respectively.

5.1.3. Co-and Post-seismic stress changes (Mw 6.0 1893 Earthquake)

The 1893- Ghazaband earthquake with Mw 6.0, occurred on 13 February, 1893 and the epicentral location (30.33823°N, 66.8479°E) of this earthquake is situated on the northern segment of the Ghazaband fault. According to the scaling law (Table 3.1), the computed results are stated in table 3.2, the rupture length, rupture width and uniform slip of 1893 Ghazaband earthquake is 7.8km, 7.2km and 0.12m respectively.

Figure 5.1(c) reports the co-seismic CFS changes at ~10km depth with an effective co-efficient of friction i.e 0.4 caused by 1893 Chaman earthquake. From the FMS of 1893 event with Mw 6.0, the receiver fault parameters are taken as strike=80°, dip= 20° and rake angle=9. This earthquake is purely a strike-slip event. Co-seismic coulomb stress changes associated with 1893 Chaman earthquake shows that this event has generated positive stress on the northern and southern lobes and negative stress on SSW-NNE lobes indicating stress shadow zones respectively (Fig. 5.1c).

We have calculated the time-dependent evolution of the stress on active faults in the region after the 1892 earthquake, since the post seismic stress after the earthquake will influence the accumulation of stress on these faults as a function of time. From figure 5.2(c), it is observed that stress accumulation on the northern segment of the Ghazaband fault is released by the preceding earthquakes with increased Δ CFS. Since the 1893 earthquake is occurred in positive lobe where the CFS value above the triggering threshold value, 0.01Mpa. Thus, it is deduced that the 1893 is triggered by the stress transfer caused by events. The maximum and minimum Δ CFS changes (combined co- and post-seismic) caused by 1893 Ghazaband earthquake are 0.2147 MPa and -0.5236MPa respectively which indicates that the maximum CFS on the rupture of 1892 event caused by the preceding earthquake is positive.

5.1.4 Co-and Post-seismic stress changes (Mw 6.0 1900 Earthquake)

The 1900- earthquake event with Mw 6.1 occurred on Ghazaband fault and the epicentral location (30.46303°N, 66.91464°E) of this earthquake is situated on the northern segment of this fault. Inferred from scaling law (Table 3.1), computed results are stated in table 3.2, the rupture length, rupture width and uniform slip of 1900 earthquake is 9.2km, 7.7km and 0.15m respectively.

Figure 5.1 (d) reports the co-seismic coulomb stress changes at ~10km depth with an effective co-efficient of friction i.e 0.4 caused by 1900 earthquake. From the focal mechanism solution of the Mw 6.1 1900 event, the receiver fault parameters are taken as strike=90°, dip= 20° and rake angle=10. Co-seismic coulomb stress changes associated with 1900 earthquake shows that this event has generated positive stress on the northern and southern lobes and negative stress on SSW -NNE lobes indicating stress shadow zones respectively (Fig. 5.1d).

We have calculated the time-dependent evolution of the stress on active faults in the region after the 1893 earthquake, since the post seismic stress after the earthquake will influence the accumulation of stress on these faults as a function of time. However, when the post-seismic viscoelastic relaxation process of 07 years between the 1900 and immediately preceding earthquake and also the duration since the inception of earthquake sequence i.e., 12 years are taken into consideration, the CFS accumulation near the epicenter of 1900 Ghazaband earthquake rises time-dependently, and reaches maximum CFS immediately before the occurrence of 1900 earthquake event Fig.5.2(d).

The maximum and minimum Δ CFS changes caused by 1900 Ghazaband earthquake are 0.07343 MPa and -11.31MPa respectively. From figure 5.1(d) and figure 5.2(d) shows that co-seismic coulomb stress changes on the rupture fault of the 1900 earthquake are less than 0.01MPa immediately after the 1893 earthquake, but are raised to more than 0.01MPa just before the occurrence of the 1900 earthquake due to post-seismic relaxation, which is about twice of the threshold for earthquake triggering (Fig. 5.2d) indicating that the 1900 Ghazaband earthquake is triggered by the preceding events.

5.1.5. Co-and Post-seismic stress changes (Mw 6.3 1908 Earthquake)

The 1908-earthquake with Mw 6.3, occurred on 05 March, 1908 and the epicentral location (30.1888°N, 67.64513°E) of this earthquake is situated on the

middle segment of the Urghargai fault. Inferred from scaling law (Table 3.1), computed results are reported in table 3.2, the rupture length, rupture width and uniform slip of 1908 earthquake is 14.3km, 9.1km and 0.25m respectively.

Figure 5.1(e) reports the co-seismic coulomb stress changes on distinct portions of the fault at the depth of 10km with an effective friction co-efficient of 0.4 caused by 1908 Ghazaband earthquake. The receiver fault parameters are taken as strike= 304° , dip= 73° and rake angle= 171 from the focal mechanism solution of the Mw 6.3 1908 event. Co-seismic coulomb stress changes associated with 1908 earthquake shows that this event has generated positive stress on the NW-SE and SW-NE and negative stress on NS and EW lobes indicating stress shadow zones respectively (Fig. 5.1e).

We have calculated the time-dependent evolution of the stress on active faults in the region after the 1900 earthquake, since the post seismic stress after the earthquake will influence the accumulation of stress on these faults as a function of time. According to the numerical results, the 1908 earthquake released the accumulated Coulomb stress on the Urghargai fault, on which seismic activity has been depressed (Figure 5.2e). As a result, the 1900 Ghazaband earthquake co-seismic static and post-seismic CFS changes may weakly enhance the occurrence of the 1908 earthquake which shows that 1908 earthquake has not been triggered by any of the previous earthquakes, hence we consider this earthquake as an independent event. The maximum and minimum Δ CFS changes caused by 1908 earthquake event are 0.252 MPa and -6.769MPa respectively.

5.1.6 Co-and Post-seismic stress changes (Mw 6.2 1910 Earthquake)

The 1910- earthquake event with Mw 6.2 occurred on Nagau fault and the epicentral location (28.38722° N, 67.01847° E) of this earthquake is situated on the southern end of this fault. Inferred from scaling law (Table 3.1), computed results are stated in table 3.2, the rupture length, rupture width and uniform slip of 1910 earthquake is 12.1km,8.5km and 0.21m respectively.

Figure 5.1 (f) reports the co-seismic coulomb stress changes on distinct portions of the fault at the depth of 10km with an effective friction co-efficient of 0.4 caused by 1910 Ghazaband earthquake. The receiver fault parameters are taken as strike= 278° , dip= 78° and rake angle= -176 from the focal mechanism solution of the Mw 6.2 1910 event. Co-seismic coulomb stress changes associated with 1908 earthquake shows that this event has generated positive stress on the Northwestern and east western lobes and

negative stress on SE, NNE and NNW lobes indicating stress shadow zones respectively (Fig. 5.1f).

We have calculated the time-dependent evolution of the stress on active faults in the region after the 1908 earthquake, since the post seismic stress after the earthquake will influence the accumulation of stress on these faults as a function of time. (Fig. 5.2f). However, when the post-seismic viscoelastic relaxation process since the inception of earthquake sequence, 1888, is taken into consideration, there has been no stress accumulation on the causative fault of 1910 earthquake which indicates that it is an independent earthquake and has not been triggered by the any of the preceding events (Fig. 5.2f). The maximum and minimum Δ CFS changes caused by 1910 Ghazaband earthquake are 0.1309 MPa and -1.208 MPa respectively.

5.1.7 Co-and Post-seismic stress changes (Mw 7.2 1931 Earthquake)

This 1931- earthquake event with Mw 7.2 occurred on Ghazaband fault and the epicentral location (29.76347° N, 66.54344° E) of this earthquake is situated on the north-western segment of the Ghazaband fault. Inferred from scaling law (Table 3.1), computed results are reported in table 3.2, the rupture length, rupture width and uniform slip of 1931 earthquake is 64.2km, 15.7km and 1.57m respectively. This earthquake caused considerable damage in and around the Quetta area.

Figure 5.1 (g) reports the co-seismic CFS changes on distinct portions of the fault at the depth of 10km with an effective friction co-efficient of 0.4 caused by 1931 Ghazaband earthquake. The receiver fault parameters are taken as strike= 80° , dip= 20° and rake angle= 9 according to the fault plane solution of the Mw 7.2 1931 event. This earthquake is purely a strike-slip event. The co-seismic static stress transfer leads the CFS increment on its northeastern and southwestern part and to CFS decrement on NNE -SSW part respectively (Fig. 5.1g).

We have calculated the time-dependent evolution of the stress on active faults in the region after the 1910 earthquake, since the post seismic stress after the earthquake will influence the accumulation of stress on these faults as a function of time. However, when the post-seismic viscoelastic relaxation process since the inception of earthquake sequence, 1888, is taken into consideration, the CFS accumulation on the epicenter of 1931 Ghazaband earthquake is raised time-dependently, and reaches maximum CFS immediately before the occurrence of 1931 earthquake event (Fig. 5.2g).

From (fig. 5.2g), it has been noted that accumulation of stress on the northwestern segment of the Ghazaband fault is released by the preceding earthquakes with increased Δ CFS which indicates the maximum CFS is above the threshold values in and around the epicenter of the 1931 earthquake. It shows that the 1931-Ghazaband earthquake is triggered by the preceding events. The maximum and minimum Δ CFS changes caused by 1931 Ghazaband earthquake are 1.543 MPa and -21.16 MPa respectively.

Figure 5.1(g) and figure 5.2(g) show that co-seismic coulomb stress changes on the rupture fault of the 1931 earthquake are less than 0.01MPa immediately after the 1910 earthquake, but is raised to more than the threshold value, 0.01MPa, just before the occurrence of the 1931 earthquake due to post-seismic relaxation (Fig 5.2g).

5.1.8. Co-and Post-seismic stress changes (Mw 7.4 1935 Earthquake)

The 1935- earthquake event with Mw 7.4 occurred on Ghazaband fault and the epicentral location (29.56538° N, 66.44589° E) of this earthquake is situated on the north-western segment of the Ghazaband fault. Inferred from scaling law (Table 3.1), computed results are stated in table 3.2, the rupture length, rupture width and uniform slip of 1935 earthquake is 84.3km, 17.3km and 2.19m respectively.

Figure 5.1 (h) reports the co-seismic CFS on distinct portions of the fault at the 10km depth with an effective friction co-efficient of 0.4 caused by 1935 Ghazaband earthquake. The receiver fault parameters were taken as strike= 33° , dip= 68° and rake angle= 124 from the focal mechanism solution of the Mw 7.4 1935 event. This earthquake is purely a strike-slip event. Co-seismic coulomb stress changes associated with 1935 earthquake shows that this event has generated positive stress on the NE-SW lobes and negative stress on NNE—SSW lobes indicating stress shadow zones respectively (Fig. 5.1h).

We have calculated the time-dependent evolution of the stress on active faults in the region after the 1931 earthquake, since the post seismic stress after the earthquake will influence the accumulation of stress on these faults as a function of time. From fig. 5.2(h) it can be observed that the epicentral location of 1935 earthquake event exhibit stress shadow zone which indicates that it has not been triggered by any of the preceding events and is considered as an independent event. The maximum and minimum Δ CFS

changes caused by 1935 Ghazaband earthquake are 6.446 MPa and -25.66 MPa respectively.

5.1.9. Co-and Post-seismic stress changes (Mw 6.2 1966 Earthquake)

The 1966-earthquake with Mw 6.2, occurred on 01 August, 1966 and the epicentral location (29.89847° N, 68.50742° E) of this earthquake is situated on the southeastern segment of the Karahi thrust. Inferred from scaling law (Table 3.1), computed results are reported in table 3.2, the rupture length, rupture width, 8.2km and uniform slip of 1966 earthquake is 11.1km and 0.57m respectively.

Figure 5.1 (i) reports the co-seismic CFS changes on distinct portions of the fault at the depth of 10km with an effective friction co-efficient of 0.4 caused by 1966 earthquake. The receiver fault parameters were taken as strike= 204.8° , dip= 42.7° and rake angle= 62.6 from the focal mechanism solution of the Mw 6.2 1966 event. Co-seismic coulomb stress changes associated with 1966 earthquake shows that this event has generated positive stress on the WNW-ESE lobes and negative stress on SW-NS lobes indicating stress shadow zones respectively (Fig. 5.1i)

We have calculated the time-dependent evolution of the stress on active faults in the region after the 1935 earthquake, since the post seismic stress after the earthquake will influence the accumulation of stress on these faults as a function of time. The co-seismic static and post-seismic coulomb failure stress changes caused by 1935 Ghazaband earthquake may weakly enhance the occurrence of 1966- earthquake event according to numerical results. From figure 5.2(i), it is observed that there is no stress accumulation released by the any of previous earthquakes. Hence, the 1966 earthquake is also considered as an independent event, not triggered by any of the preceding events. The maximum and minimum Δ CFS changes caused by 1966 earthquake event are 1.054 MPa and -1.273 MPa respectively.

5.1.10. Co-and Post-seismic stress changes (Mw 6.8 1975a Earthquake)

Since 02 earthquake occurred in 1975 in our selected sequence of earthquakes. So, we named them 1975a and 1975b respectively. The 1975a- earthquake event with Mw 6.8 occurred on Ghazaband fault and the epicentral location (30.24115° N, 66.27456° E) of this earthquake is situated on the southwestern segment of this fault. Inferred from scaling law (Table 3.1), computed results are reported in table 3.2, the

rupture length, rupture width and uniform slip of 1975a earthquake is 30.3km, 11.9km and 0.63m respectively.

Figure 5.1 (j) reports the co-seismic CFS changes on distinct portions of the fault at the depth of 10km with an effective friction co-efficient of 0.4 caused by 1975a Ghazaband earthquake. The receiver fault parameters were taken as strike=80°, dip=20° and rake angle=0.34 from the focal mechanism solution of the Mw 6.8 1975a event. From fig 5.1 (j), it is observed that the state of the stress field has been changed significantly due to co-seismic changes caused by 1975a earthquake. The co-seismic static stress transfer leads the CFS increment on the NS and EW ends of the rupture fault and CFS decrement on the SE and NNW lobes respectively.

We have calculated the time-dependent evolution of the stress on active faults in the region after the 1966 earthquake, since the post seismic stress after the earthquake will influence the accumulation of stress on these faults as a function of time. However, when the post-seismic viscoelastic relaxation process since the inception of earthquake sequence, 1888, is taken into consideration, the CFS accumulation near the epicenter of 1975a Ghazaband earthquake is raised time-dependently, and reaches maximum CFS immediately before the occurrence of 1975a earthquake event (Fig. 5.2j)

The 1935 event which ruptured the Ghazaband fault eventually raised the maximum and average Δ CFS 0.518Mpa and -13.91 MPa respectively on the rupture segment of impending 1975a earthquake (fig 5.2j). It indicates CFS is above threshold value in the epicentral vicinity of 1975a. Thus, it is deduced that 1975a earthquake is triggered by the previous earthquakes.

5.1.11. Co-and Post-seismic stress changes (Mw 6.6 1975b Earthquake)

The 1975b- earthquake event with Mw 6.6 occurred on Ghazaband fault 12 hours later after the 1975a earthquake. The epicentral location (30.12693°N, 21032°E) of this earthquake is situated on the southwestern segment of Ghazaband fault. Inferred from scaling law (Table 3.1), computed results are reported in table 3.2, the rupture length, rupture width and uniform slip of 1975b earthquake is 21.6km, 10.5km and 0.42m respectively.

Figure 5.1 (k) reports the co-seismic coulomb stress changes on distinct portions of the fault 10km depth with an effective friction co-efficient of 0.4 caused by 1975b

Ghazaband earthquake. The receiver fault parameters are taken as strike= 80° , dip= 20° and rake angle= 10 from the focal mechanism solution of the Mw 6.6 1975b event. This earthquake is purely a strike-slip event. From fig 5.1 (k), it is observed that, the state of the stress field due to co-seismic changes caused by 1975b earthquake has been changed significantly on either terminus of ruptured segment. The co-seismic static stress transfer leads the CFS increment on the north and south ends of the rupture fault (fig 5.1k).

We have calculated the time-dependent evolution of the stress on active faults in the region after the 1975a earthquake, since the post seismic stress after the earthquake will influence the accumulation of stress on these faults as a function of time. However, with the post-seismic viscoelastic relaxation process, the CFS accumulation near the epicenter of 1975b Ghazaband earthquake is raised in a time-dependent manner and reaches maximum CFS immediately before the occurrence of 1975b earthquake event (Fig. 5.2k), and had advanced occurrence of 1975b earthquake. Because the 1935 event occurred in the southern positive CFS lobe by the 1892 earthquake, the 1935 event created a stress shadow zone on the southern lobe of the 1975 earthquake. It can be also observed that the Chaman fault system stress orientation was largely influenced by the 1935 Ghazaband earthquake. The maximum and minimum Δ CFS changes caused by 1975b earthquake are 1.002 and -4.3491Mpa respectively.

5.1.12. Co-and Post-seismic stress changes (Mw 6.2 1990 Earthquake)

The 1990- earthquake event with Mw 6.2 occurred on Ghazaband fault. The epicentral location (28.97825° N, 66.21032° E) of this earthquake is situated on the southern segment of this fault. Inferred from scaling law (Table 3.1), computed results are reported in table 3.2, the rupture length, rupture width and uniform slip of 1990 earthquake is 10.9km, 8.2km and 0.18m respectively.

Figure 5.1(l) reports the co-seismic CFS on distinct portions of the fault at the 10km depth with an effective friction co-efficient of 0.4 caused by 1990 Ghazaband earthquake. The receiver fault parameters are taken as strike= 278° , dip= 78° and rake angle= -176 from the focal mechanism solution of the Mw 6.2 1990 event. This earthquake is purely a strike-slip event. The co-seismic static stress transfer leads the CFS increment on the NS and EW ends of the rupture fault and CFS decrement on the

SE and NNW segments. The 1990 earthquake occurred on the southern-stress positive lobe of the 1935 event's rupture segment where the maximum and minimum (combine co- and post-seismic Δ CFS changes) are 0.2581Pa and -2.051Mpa respectively.

From fig 5.1(l) it is observed that the state of the stress field due to co-seismic changes caused by 1990 event has been changed significantly. The southern zone of the earthquake exhibits stress shadow zone during co-seismic state.

We have calculated the time-dependent evolution of the stress on active faults in the region after the 1975 earthquake, since the post seismic stress after the earthquake will influence the accumulation of stress on these faults as a function of time. However, when the post-seismic viscoelastic relaxation process since the inception of earthquake sequence, 1888, is taken into consideration, the CFS accumulation in the epicentral vicinity of 1990 Ghazaband earthquake is raised time-dependently, and reaches maximum CFS before the occurrence of 1990 earthquake event. It eventually caused the advance occurrence of 1990 earthquake (Fig. 5.2 (l)).

5.1.13. Co-and Post-seismic stress changes (Mw 7.1 1997 Earthquake)

The 1997 earthquake event with Mw 7.1 occurred in the kirthar-sulaiman shear zone near the town of Harnai ~60km ENE to Sibi and ~100km SE to Quetta. The epicenter of 1997 earthquake was located at 29.80805N and 68.26472E with a depth of less than 10km. Inferred from scaling law (Table 3.1), computed results are reported in table 3.2, the rupture length, rupture width and uniform slip of 1997 earthquake is 50.6km, 14,4km and 1.17m respectively.

Figure 5.1 (m) reports the co-seismic CFS changes on distinct portions of the fault 10km depth with an effective friction co-efficient of 0.4 caused by 1997 Harnai earthquake. The receiver fault parameters are taken as strike=85°, dip= 77° and rake angle=82 from the focal mechanism solution of the Mw 7.1 1997 event. This earthquake is essentially a thrust event with some strike-slip component. Co-seismic coulomb stress changes associated with 1997 Harnai earthquake shows that this event have generated positive stress on the North southern and east western lobes and negative stress on SE, NNE and NNW lobes indicating stress shadow zones respectively (Fig. 5.1m).

We have calculated the time-dependent evolution of the stress on active faults in the region after the 1990 earthquake, since the post seismic stress after the earthquake will influence the accumulation of stress on these faults as a function of time. The numerical findings show that the co-seismic static and post-seismic CFS changes caused by 1990 Ghazaband earthquake may weakly enhance the occurrence of 1997-earthquake event. From figure 5.2 (m) it is observed that the epicentral location of 1997 earthquake exhibits stress shadow zone. Thus, it is deduced that 1997 earthquake was an independent event, not triggered by any of the previous earthquakes. The maximum and minimum Δ CFS changes (combined co- and post-seismic) caused by 1997 earthquake event are 1.33 MPa and -14.52 respectively.

5.1.14. Co-and Post-seismic stress changes (Mw 6.4 2008a and 2008b Earthquakes)

Since 02 earthquake occurred in 2008 in our selected sequence of earthquakes. So, we named them 2008a and 2008b respectively. On 28 October 2008, 02 main earthquakes with similar focal depth i.e 10km, identical magnitude (Mw=6.4) and fault plane solutions (right-lateral strike-slip) shook the ziarat town and surrounding areas in Sulaiman fold-and-thrust belt of NE Baluchistan, Pakistan. It was later named as Ziarat doublet earthquake (ZDE). The epicenter of the 2008a and 2008b earthquakes were located at 30.698N ,67.49285E and 30.58379°N, 67.5214°E respectively.

The ZDE is the strongest and deadliest in Baluchistan since 27 February 1997, Harnai earthquake of magnitude 7.0 that caused widespread destruction in the region. These earthquakes are located along 80km east of the 650km long Chaman fault. FMS of ZDE show activation of the northwest striking right-lateral strike slip fault named as Urghargai fault, in the Gogai Nappe zone, northeastern Baluchistan. Inferred from scaling law (Table 3.3), computed results are stated in table 3.2, the rupture length, rupture width and uniform slip of 2008a earthquake is 15.3km, 9.3km and 0.28m respectively.

Figure 5.1 (n) reports the co-seismic CFS changes on distinct portions of the fault at 10km depth with an effective friction co-efficient of 0.4 caused by 2008a Ziarat earthquake. The receiver fault parameters are taken as strike=304°, dip= 73° and rake angle=171 from the focal mechanism solution of the Mw 6.4 2008a event. This earthquake is purely a strike-slip event. The co-seismic static stress transfer leads the

CFS increment on the NNW-SSE and NE-SW ends of the rupture fault and CFS decrement on the NW and EW lobes respectively (Fig 5.1n).

We have calculated the time-dependent evolution of the stress on active faults in the region after the 1997 earthquake, since the post seismic stress after the earthquake will influence the accumulation of stress on these faults as a function of time. However, when the post-seismic viscoelastic relaxation process since the inception of earthquake sequence, 1888, is taken into consideration, the CFS accumulation in the epicentral vicinity of 2008a earthquake is raised time-dependently, and reaches beyond the threshold value before the occurrence of 2008a earthquake event (Fig. 5.2n). It eventually triggered the 2008a earthquake. The maximum and minimum (combine co- and post-seismic Δ CFS changes) are 0.2581MPa and 2.051MPa respectively. From figure 5.2n it is observed that the epicentral location of 2008a earthquake exhibits highly stressed region which shows that it has been triggered by the preceding events.

After 12 hours another earthquake occurred with a magnitude identical to the 1st event i.e., Mw 6.4 occurred about 25km south-east to the 2008a event. The epicenter of 2008b earthquake was located at 30.58379°N and 67.5214°E respectively. Inferred from scaling law (Table 3.3), the rupture length, rupture width and uniform slip of 2008b earthquake is 15.3km, 9.3km and 0.28m respectively.

Figure 5.1 (o) reports the co-seismic CFS changes on distinct portions of the fault at the depth of 10km with an effective friction co-efficient of 0.4 caused by 2008b Ziarat earthquake. The receiver fault parameters are taken as strike=324°, dip= 68° and rake angle= -178 from the FMS of the Mw 6.4 2008b event. The co-seismic static stress transfer leads the CFS increment on the NNW-SSE and NE-SW ends of the rupture fault and CFS decrement on the NW and EW lobes respectively (Fig 5.1o).

We have calculated the time-dependent evolution of the stress on active faults in the region after the 1997 earthquake, since the post seismic stress after the earthquake will influence the accumulation of stress on these faults as a function of time. Due to post-seismic time-dependent viscoelastic relaxation, CFS accumulation near the epicenter of 2008b earthquake is raised time-dependently, and reaches beyond the threshold value 0.01MPa before the occurrence of 2008b earthquake event Fig. 5.2(o). It eventually triggered the 2008b earthquake. The maximum and minimum (combine co- and post-seismic Δ CFS changes) are 0.2284MPa and -5.009MPa respectively. From

figure 5.2(o), it is observed that the epicentral location of 2008b earthquake exhibits highly stressed region which shows that it has been triggered by the preceding events respectively.

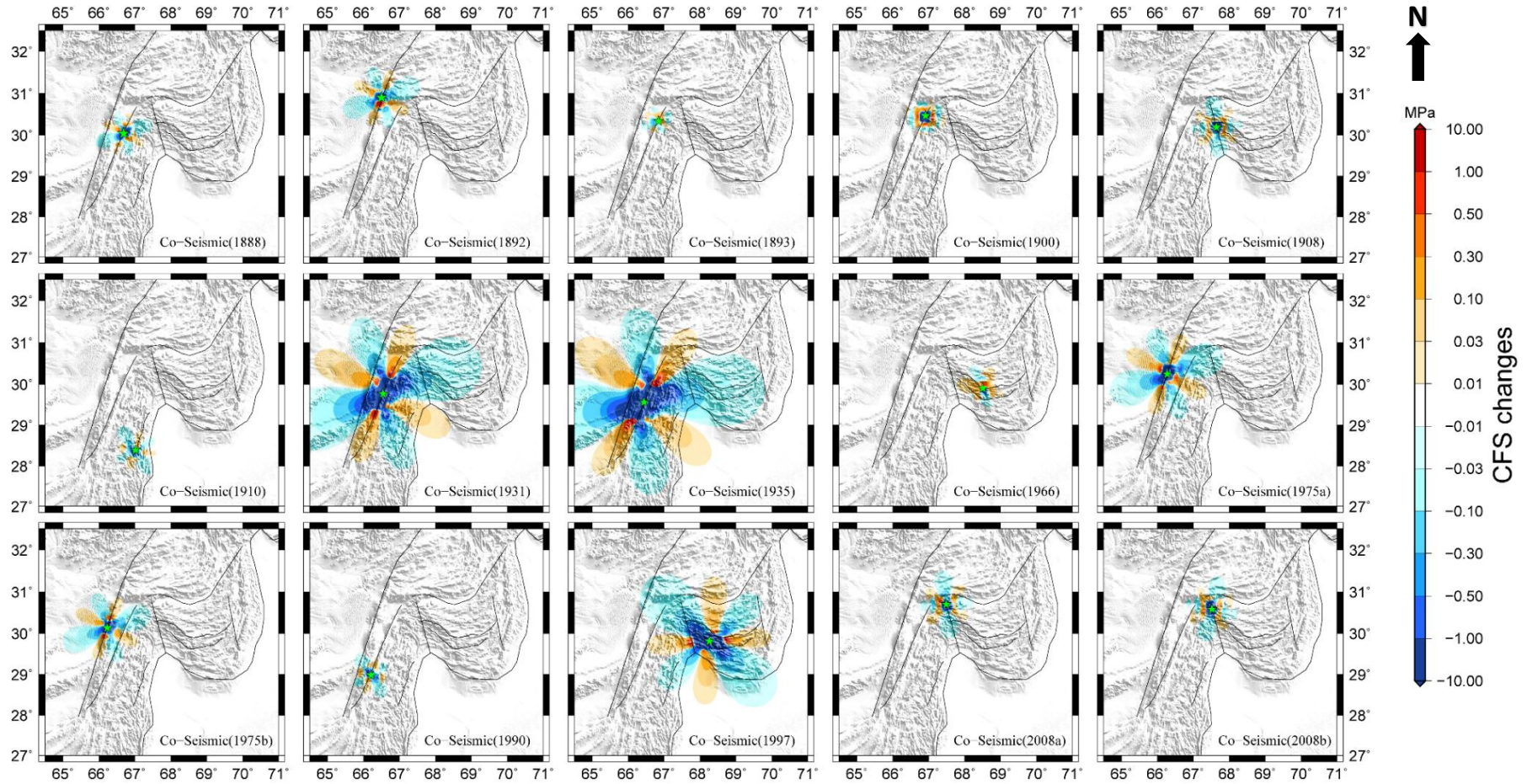


Figure 5.1. (a-o) The Coseismic Coulomb stress changes caused by the 1888-2008 earthquake sequence. Active faults in the study are indicated by black lines. The Green star indicates the portion of the current earthquake rupture in the area.

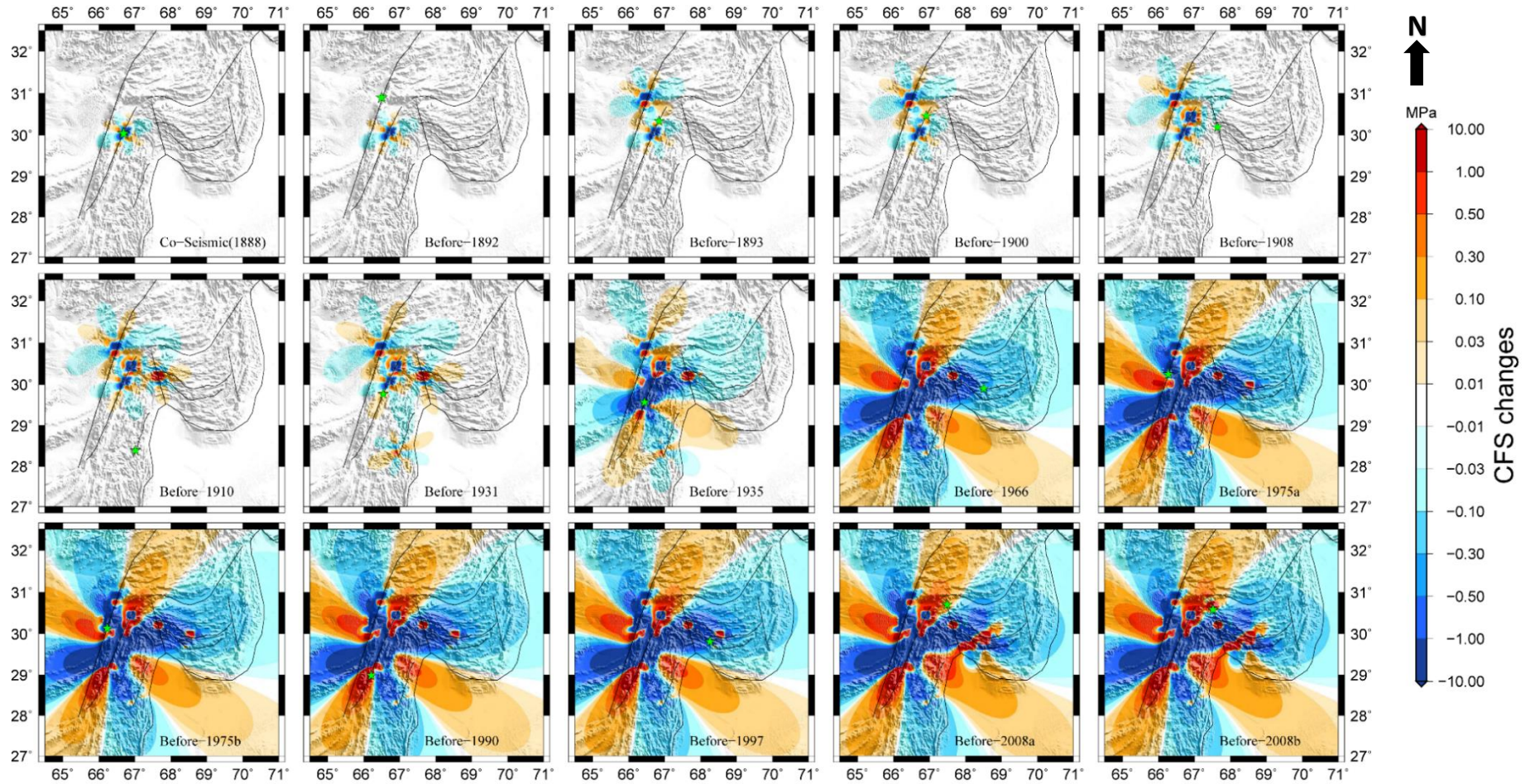


Figure 5.2. (a-o) The CFS evolution at the 10km depth since 1888. Active faults in the study area are indicated by the black lines. The Green star indicates the portion of next earthquake rupture. The Δ CFS is depicted in each snapshot series just before the subsequent earthquake

5.2. Robustness of Numerical Results

To verify the robustness of our results, we conducted numerous simulations with different combinations of following two factors:

- a. Co-efficient of friction.
- b. Effect of viscosity.

Table 5.2 reports the parametric values of co-efficient of friction, lower crust and upper mantle viscosities opted for simulations in order to verify the robustness of our results.

5.2.1. Co-efficient of friction (μ')

The selection of an appropriate value for the effective co-efficient of friction (μ') is of minor importance for the model because it regulates just the contribution of the normal stress to the CFS (King et al., 1994). The μ' varies depending on the fault type, with higher values (0.6-0.8) for thrust and normal faults and lower values (0.2-0.4) for strike-slip faults (Xiong et al., 2010). As previously mentioned, a moderate value of 0.4 is used in the numerical calculations. Numerical studies reveal that for different values of co-efficient of friction (μ'), the viscosity of lower crust and upper mantle, there are some minor differences in the computed stress. The results are reported in (Figs 5.3-5.16).

5.2.2. Viscosity

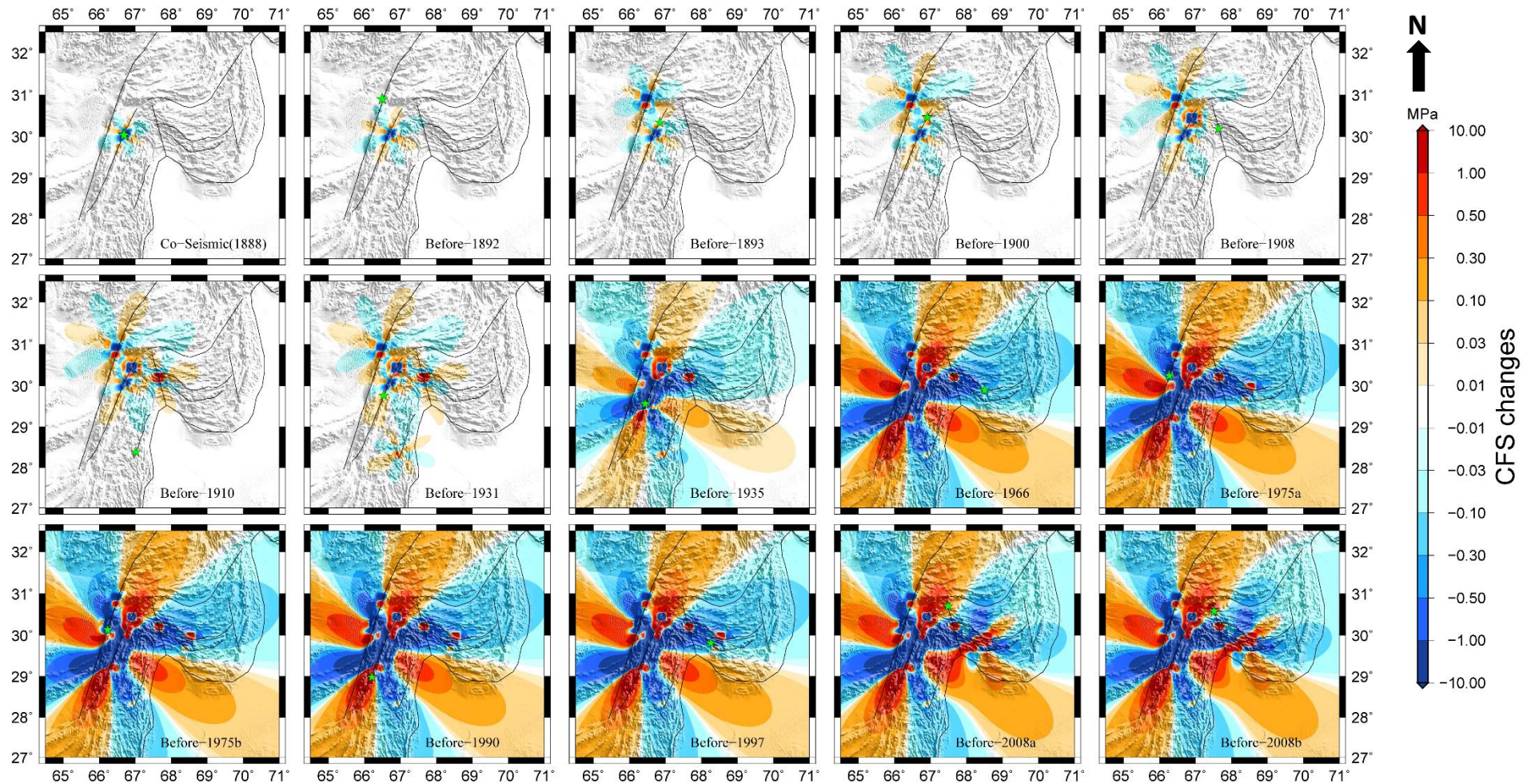
The viscosities of the lower crust and upper mantle are crucial in computing the time-dependent stress-field as viscoelastic relaxation has been included in the calculations, and also effected the speed of time-dependent relaxation. We used viscosities in this study that are consistent with the findings of earlier studies on post-seismic deformation. (Ryder et al., 2007; Shao et al., 2008). The crust and upper mantle viscosities are not adequately constrained due to a lack of continuous observation of post-seismic deformation in the examined region. As a result, we experimented with different values of viscosity to ensure the durability of the results.

Five different simulations with different values of effective co-efficient of friction and lower crust and upper mantle viscosities have been conducted as shown in Table 5.2. The results associated with simulation I have are illustrated in figures

5.3(a-o), 5.4(a-o) and 5.5(a-o), with simulation II in figures 5.2(a-o), 5.6(a-o) and 5.7(a-o), with simulation III in figures 5.8(a-o), 5.9(a-o) and 5.10(a-o), with simulation IV are showed in figures 5.11(a-o), 5.12(a-o) and 5.13(a-o) and with simulation V results are shown in figures 5.14(a-o), 5.15(a-o) and 5.16(a-o) respectively.

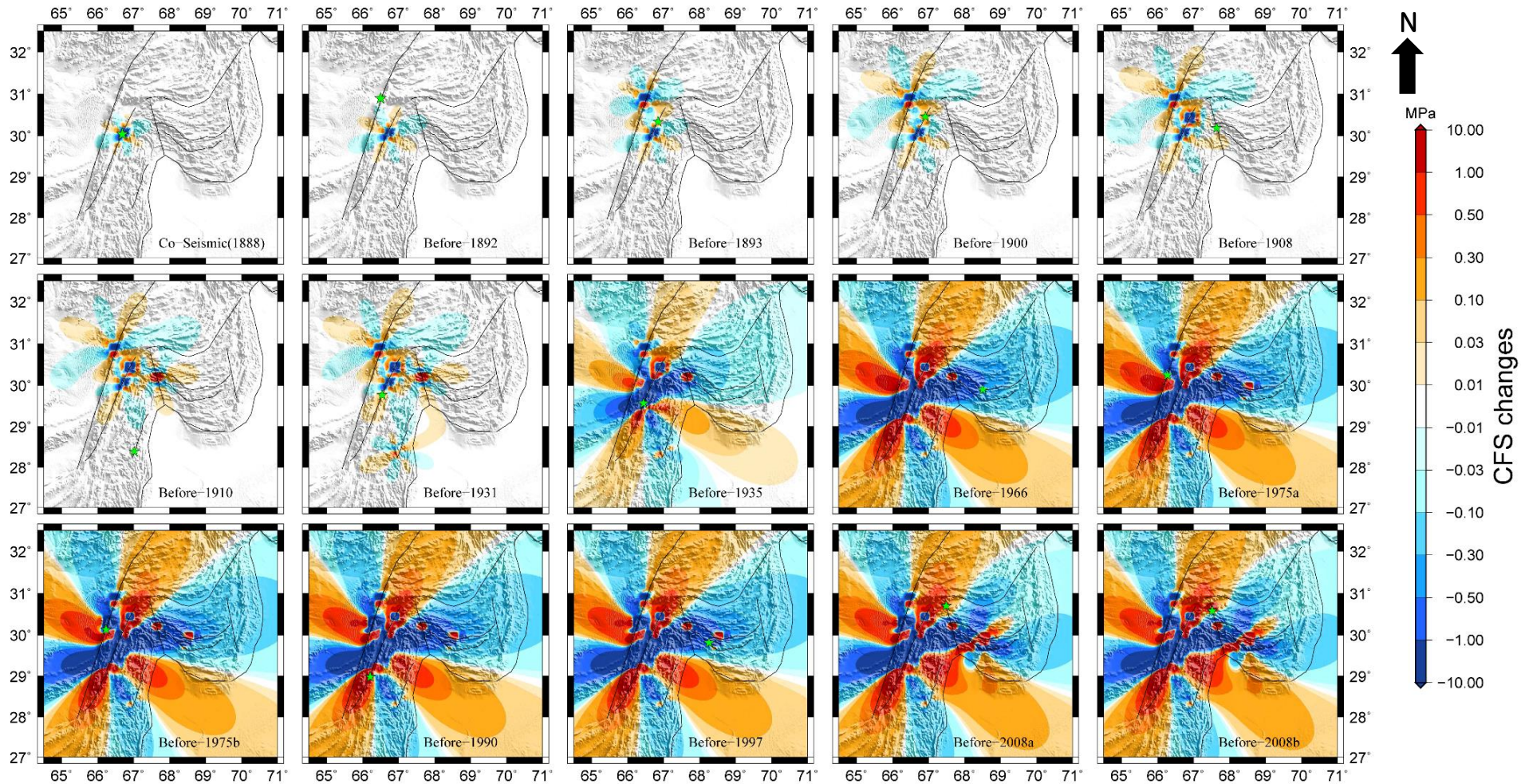
Table 5.1 Simulations of result with various values of viscosity and friction

Simulations	Viscosity	Friction
I.	Lower Crust = 1×10^{18} Pa s	$\mu' = 0.2$
	Upper Mantle = 1×10^{18} Pa s	$\mu' = 0.4$ $\mu' = 0.6$
II.	Lower Crust = 1×10^{19} Pa s	$\mu' = 0.2$
	Upper Mantle = 1×10^{19} Pa s	$\mu' = 0.4$ $\mu' = 0.6$
III.	Lower Crust = 1×10^{19} Pa s	$\mu' = 0.2$
	Upper Mantle = 1×10^{20} Pa s	$\mu' = 0.4$ $\mu' = 0.6$
IV.	Lower Crust = 1×10^{18} Pa s	$\mu' = 0.2$
	Upper Mantle = 1×10^{19} Pa s	$\mu' = 0.4$ $\mu' = 0.6$
V.	Lower Crust = 1×10^{20} Pa s	$\mu' = 0.2$
	Upper Mantle = 1×10^{20} Pa s	$\mu' = 0.4$ $\mu' = 0.6$



$\mu' = 0.2$, η_{LC} (viscosity of lower crust) = 1×10^{18} Pa s, η_M (viscosity of upper mantle) = 1×10^{18} Pa s

Figure 5.3. (a-o) The ΔCFS evolution at the 10km depth since 1888. Active faults in the research area are indicated by black lines. The Green star indicates the portion of next earthquake rupture. The ΔCFS is depicted in each snapshot series just before the subsequent earthquake. The increased and decreased ΔCFS are represented by warm and cool tones.



$\mu' = 0.4$, η_{LC} (viscosity of lower crust) = 1×10^{18} Pa s, η_M (viscosity of upper mantle) = 1×10^{18} Pa s

Figure 5.4. (a-o) The Δ CFS evolution at the 10km depth since 1888. Active faults in the study area are indicated by black lines. Green star denotes the portion of next earthquake rupture. Each snapshot series illustrates the Δ CFS immediately before the subsequent earthquake. Warm tone and cool tone represent the increased and decreased Δ CFS respectively.

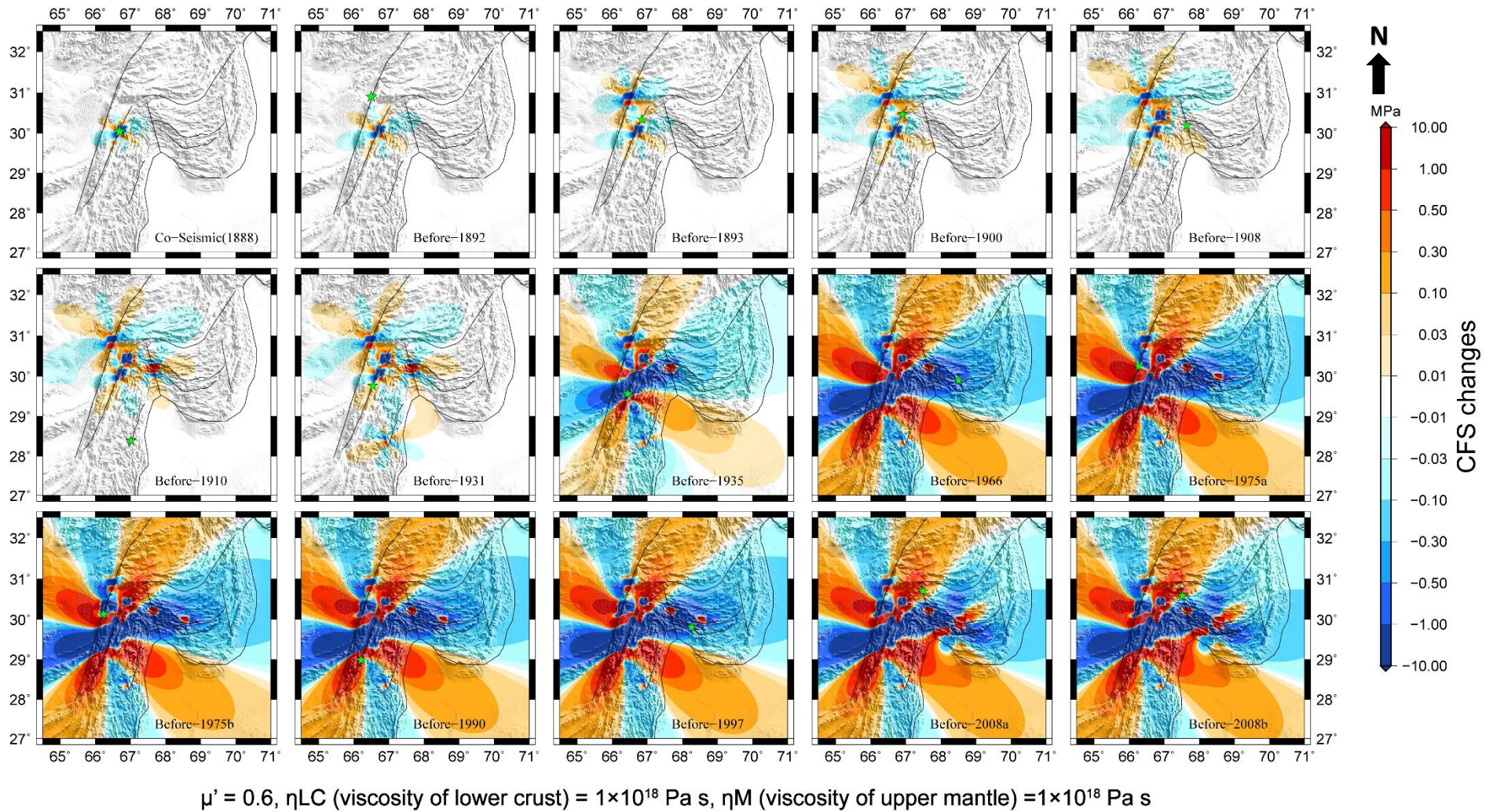
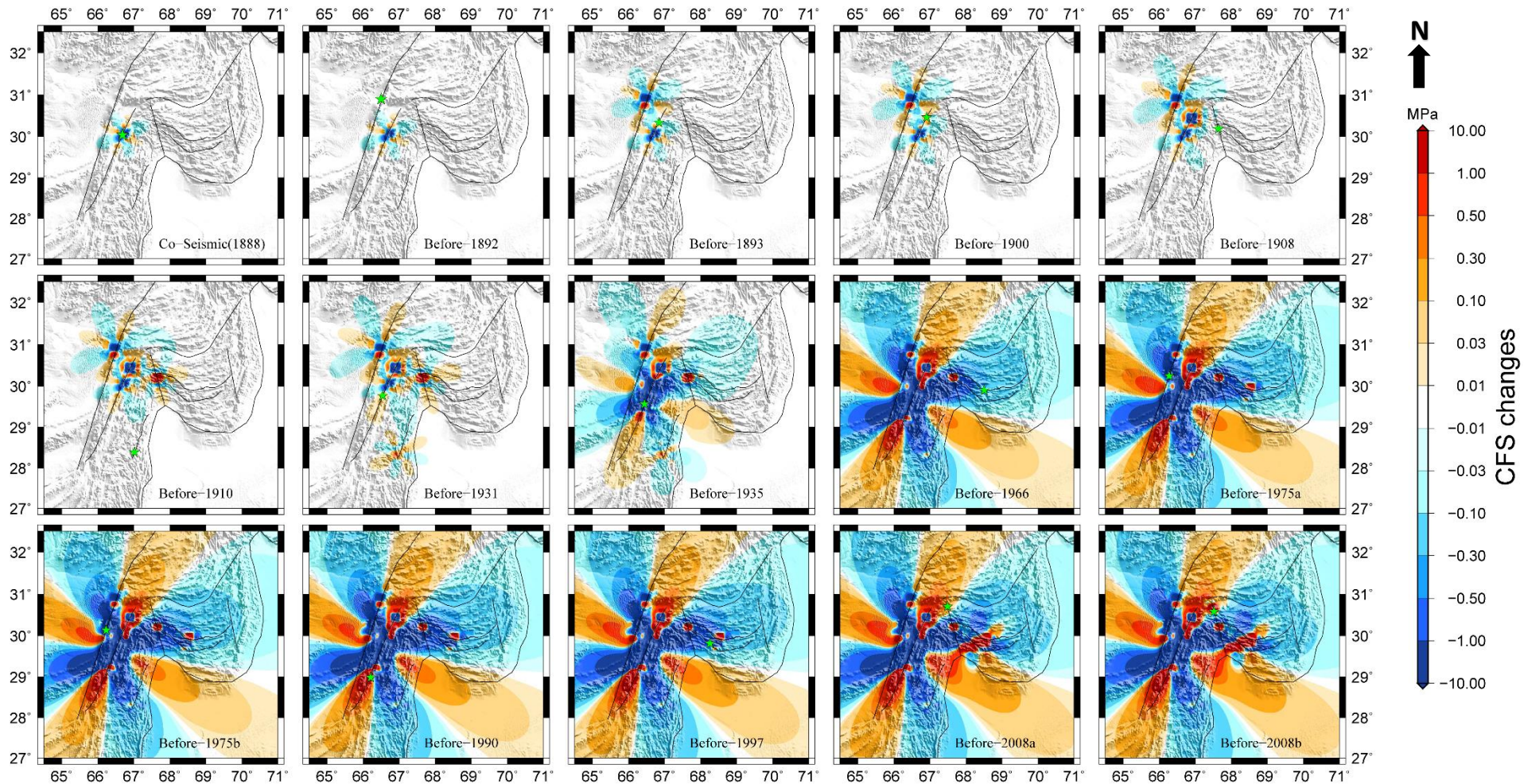


Figure 5.5. (a-o) The Δ CFS evolution at the 10km depth since 1888. Active faults in the study area are indicated by black lines. The Green star indicates the portion of next earthquake rupture. The Δ CFS is depicted in each snapshot series just before the subsequent earthquake. The increased and decreased Δ CFS are represented by warm and cool tones.

Results Associated with Simulation II



$$\mu' = 0.2, \eta_{LC} \text{ (viscosity of lower crust)} = 1 \times 10^{19} \text{ Pa s}, \eta_M \text{ (viscosity of upper mantle)} = 1 \times 10^{19} \text{ Pa s}$$

Figure 5.6. (a-o) The Δ CFS evolution at the 10km depth since 1888. Active faults in the study area are indicated by black lines. The Green star indicates the portion of next earthquake rupture. The Δ CFS is depicted in each snapshot series just before the subsequent earthquake. The increased and decreased Δ CFS are represented by warm and cool tones.

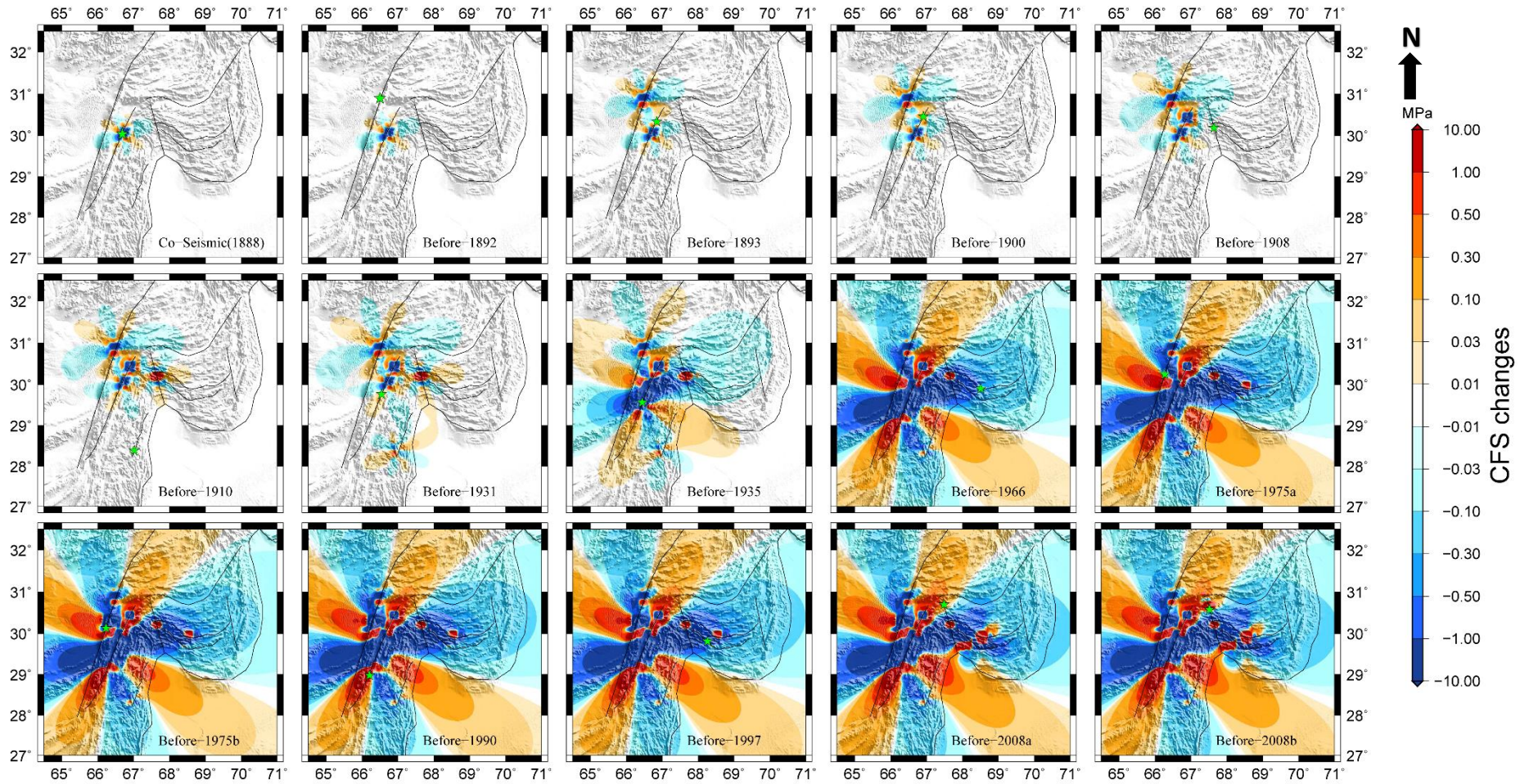


Figure 5.7. (a-o) The Δ CFS evolution at the 10km depth since 1888. Active faults in the study area are indicated by black lines. The Green star indicates the portion of next earthquake rupture. The Δ CFS is depicted in each snapshot series just before the subsequent earthquake. The increased and decreased Δ CFS are represented by warm and cool tones.

Results Associated with Simulation III

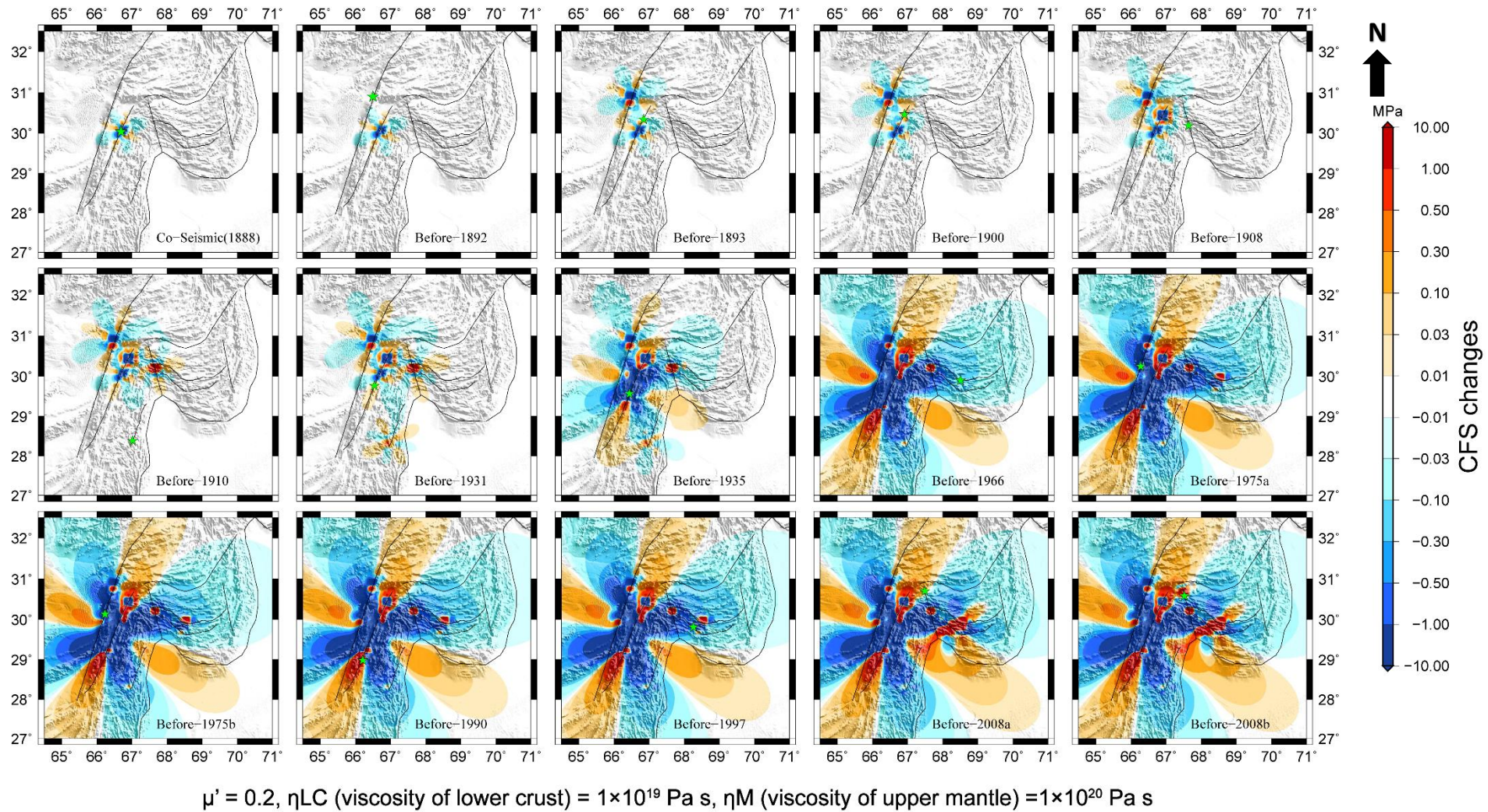
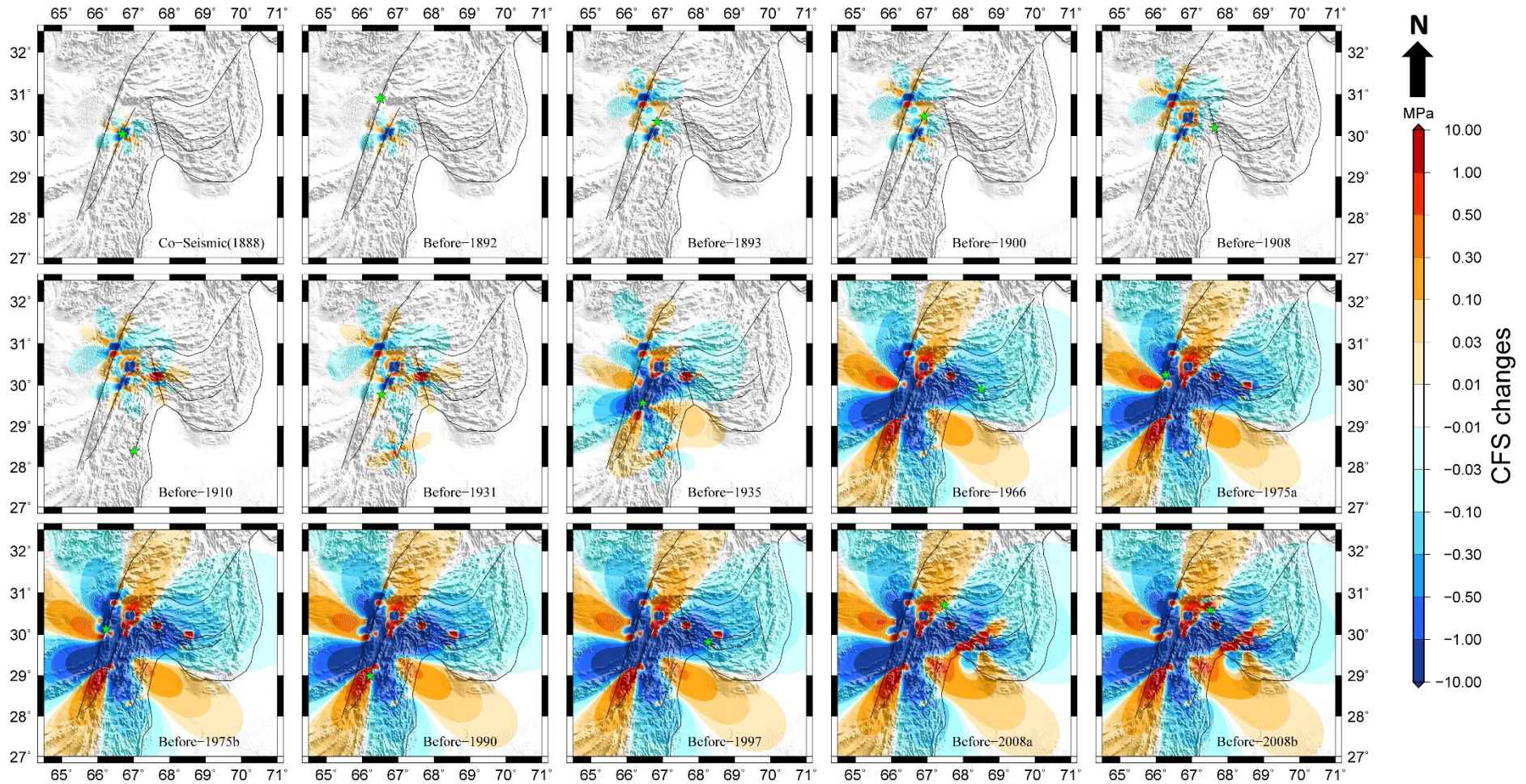


Figure 5.8. (a-o) The Δ CFS evolution at the 10km depth since 1888. Active faults in the study area are indicated by black lines. The Green star indicates the portion of next earthquake rupture. The Δ CFS is depicted in each snapshot series just before the subsequent earthquake. The increased and decreased Δ CFS are represented by warm and cool tones.



$$\mu' = 0.4, \eta_{LC} \text{ (viscosity of lower crust)} = 1 \times 10^{19} \text{ Pa s}, \eta_M \text{ (viscosity of upper mantle)} = 1 \times 10^{20} \text{ Pa s}$$

Figure 5.9. (a-o) The Δ CFS evolution at the 10km depth since 1888. Active faults in the study area are indicated by black lines. The Green star indicates the portion of next earthquake rupture. The Δ CFS is depicted in each snapshot series just before the subsequent earthquake. The increased and decreased Δ CFS are represented by warm and cool tones.

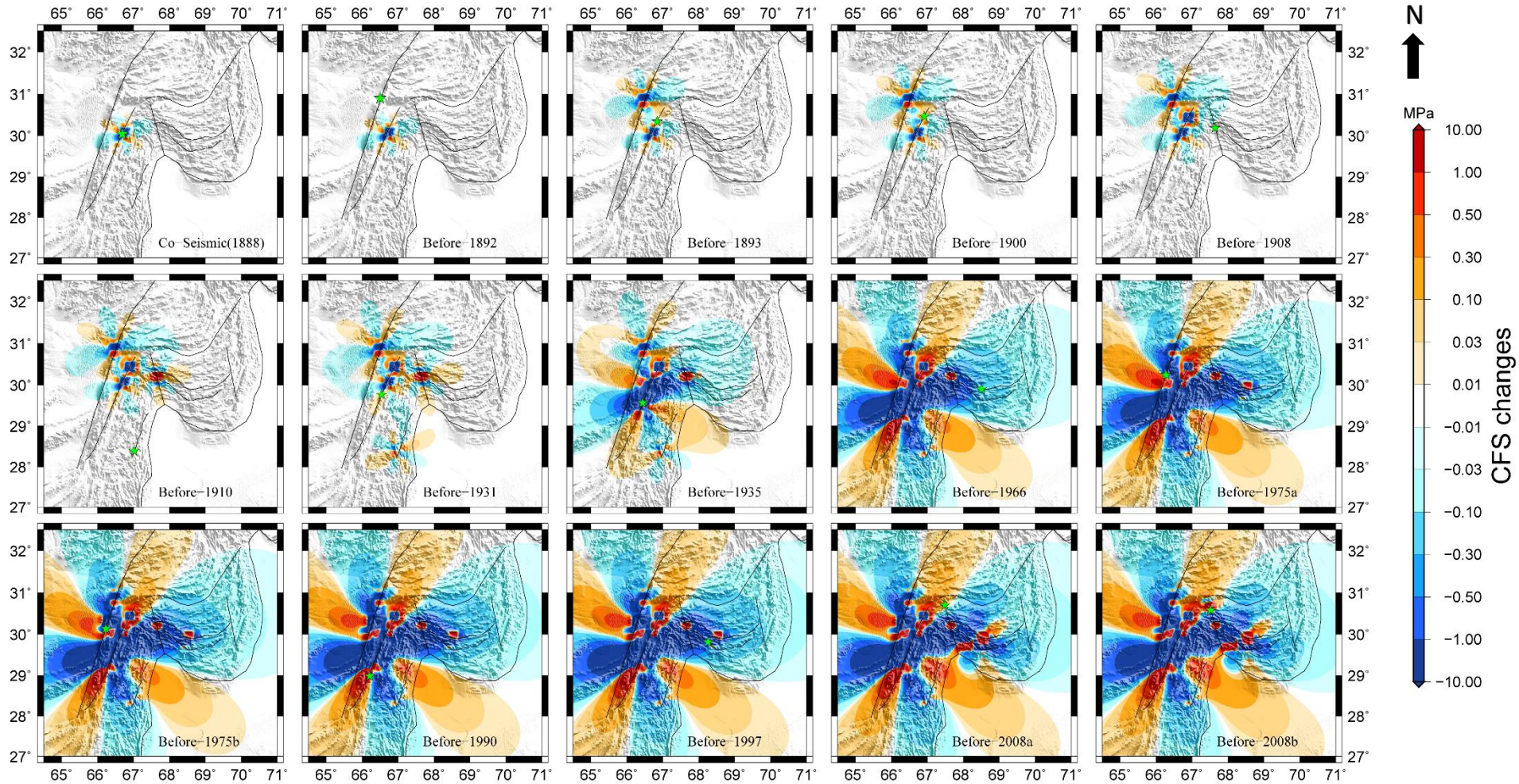


Figure 5.10. (a-o) The Δ CFS evolution at the 10km depth since 1888. Active faults in the study area are indicated by black lines. The Green star indicates the portion of next earthquake rupture. The Δ CFS is depicted in each snapshot series just before the subsequent earthquake. The increased and decreased Δ CFS are represented by warm and cool tones.

Results Associated with Simulation IV

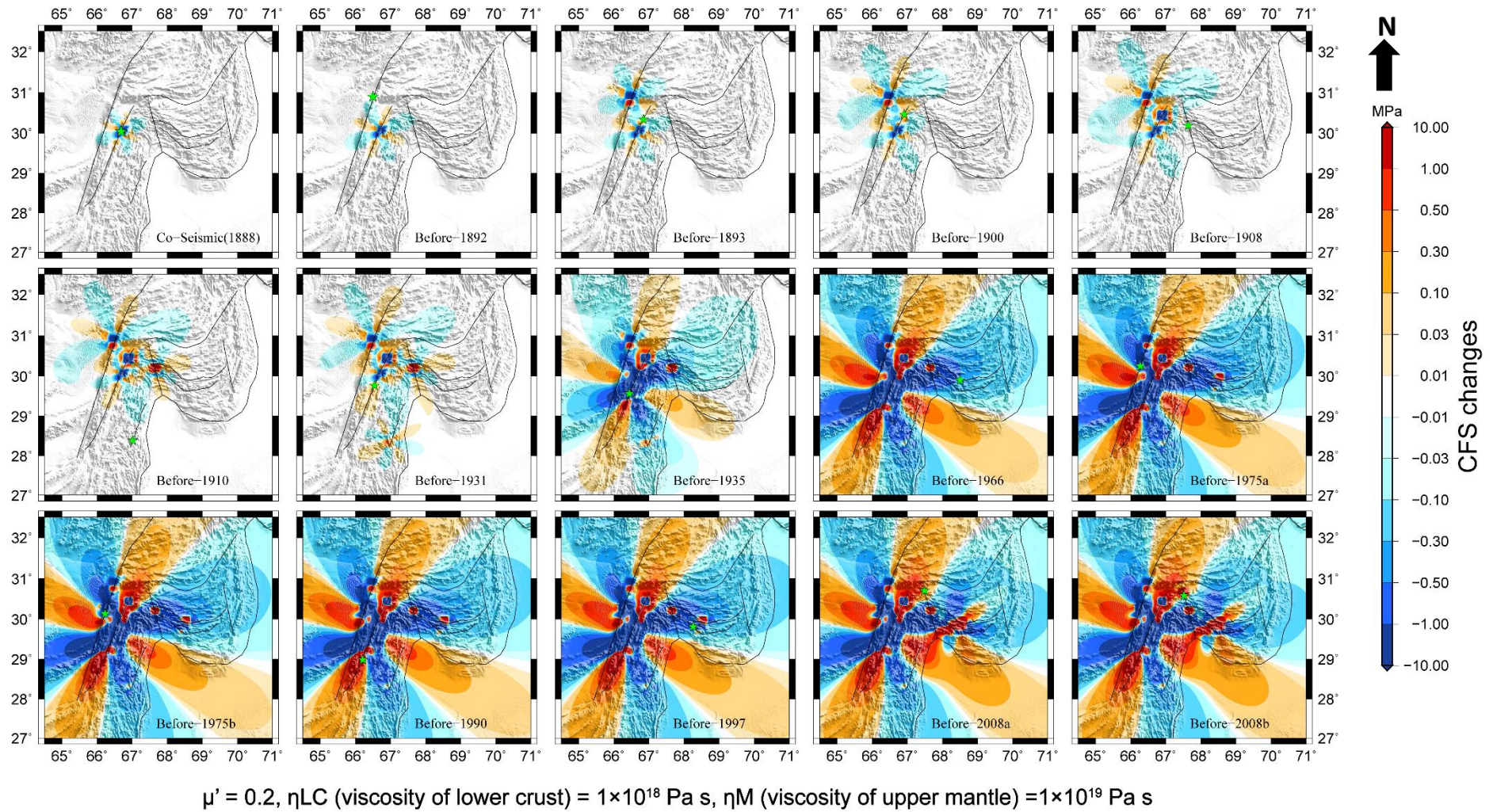


Figure 5.11. (a-o) The Δ CFS evolution at the 10km depth since 1888. Active faults in the study area are indicated by black lines. The Green star indicates the portion of next earthquake rupture. The Δ CFS is depicted in each snapshot series just before the subsequent earthquake. The increased and decreased Δ CFS are represented by warm and cool tones.

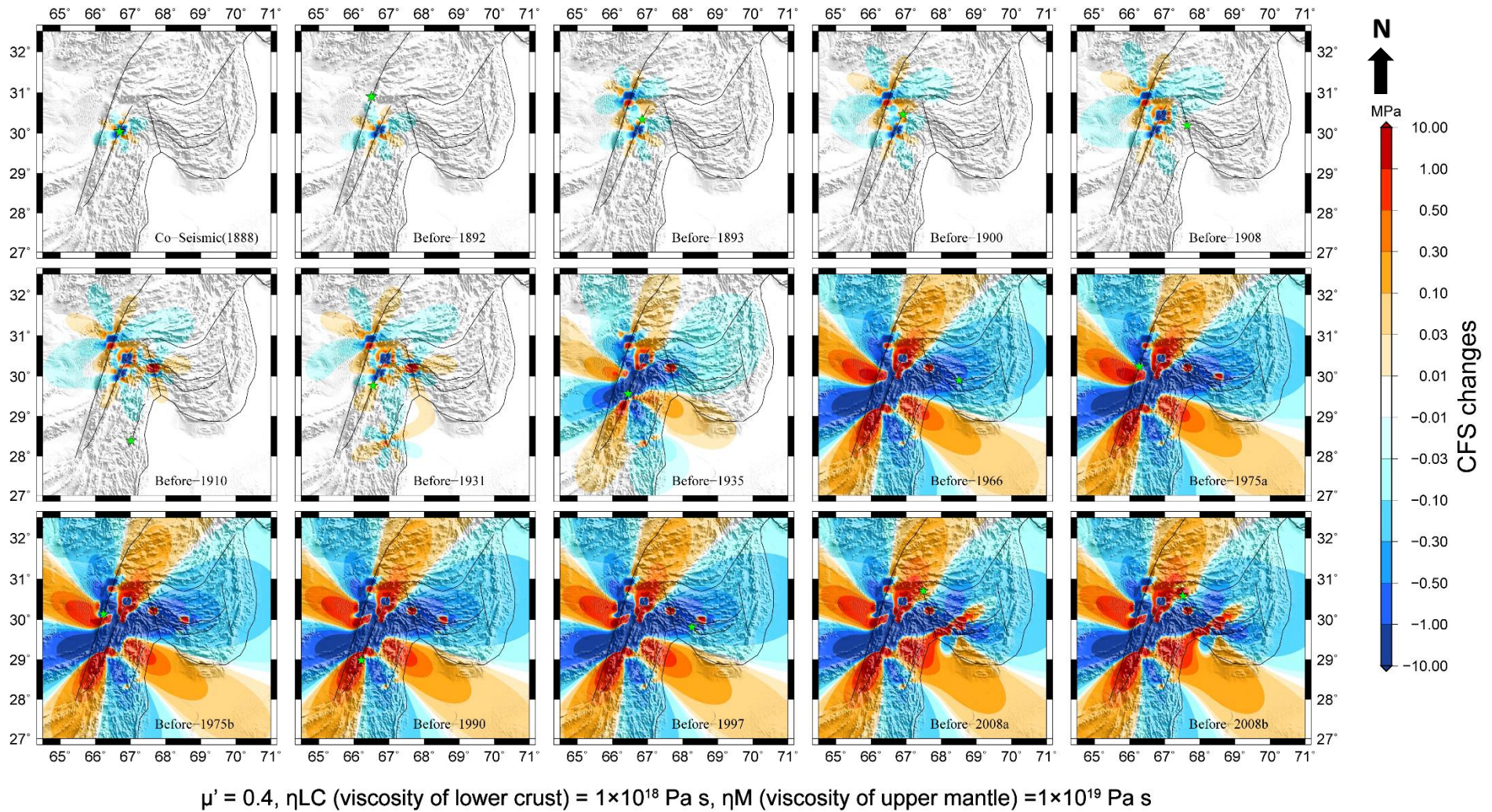


Figure 5.12. (a-o) The Δ CFS evolution at the 10km depth since 1888. Active faults in the study area are indicated by black lines. The Green star indicates the portion of next earthquake rupture. The Δ CFS is depicted in each snapshot series just before the subsequent earthquake. The increased and decreased Δ CFS are represented by warm and cool tones.

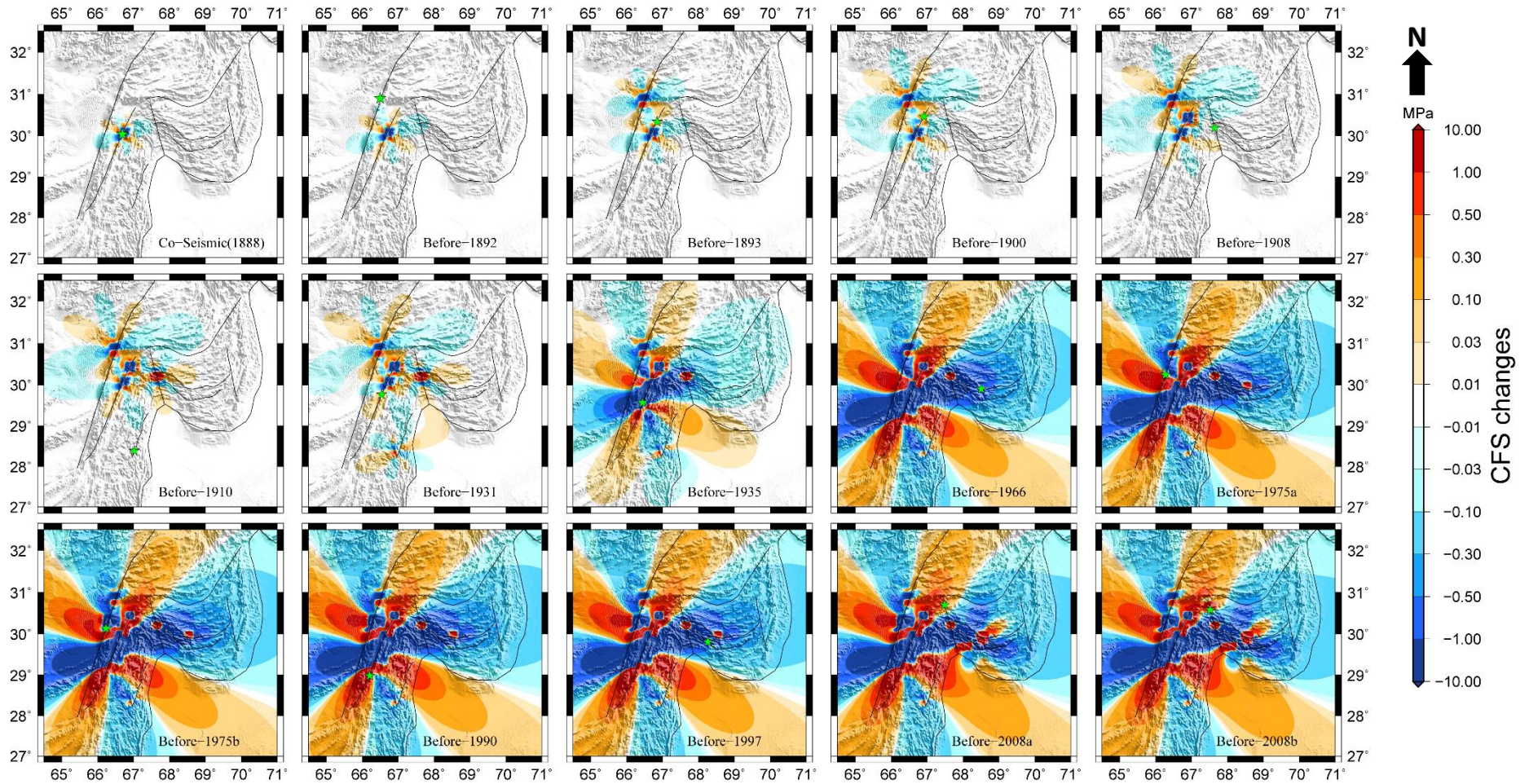


Figure 5.13. (a-o) The Δ CFS evolution at the 10km depth since 1888. Active faults in the study area are indicated by black lines. The Green star indicates the portion of next earthquake rupture. The Δ CFS is depicted in each snapshot series just before the subsequent earthquake. The increased and decreased Δ CFS are represented by warm and cool tones.

Results Associated with Simulation V

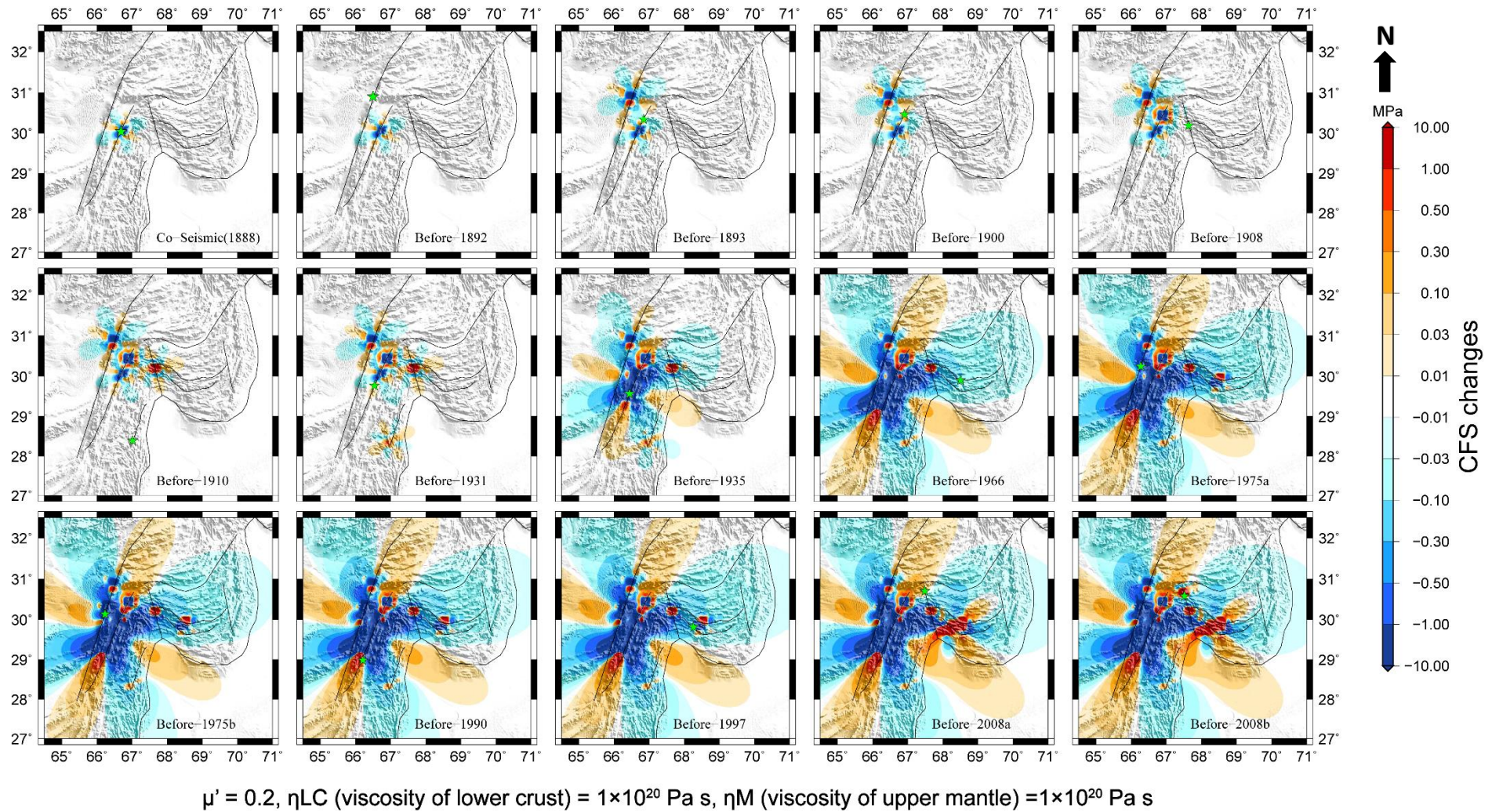


Figure 5.14. (a-o) The Δ CFS evolution at the 10km depth since 1888. Active faults in the study area are indicated by black lines. The Green star indicates the portion of next earthquake rupture. The Δ CFS is depicted in each snapshot series just before the subsequent earthquake. The increased and decreased Δ CFS are represented by warm and cool tones.

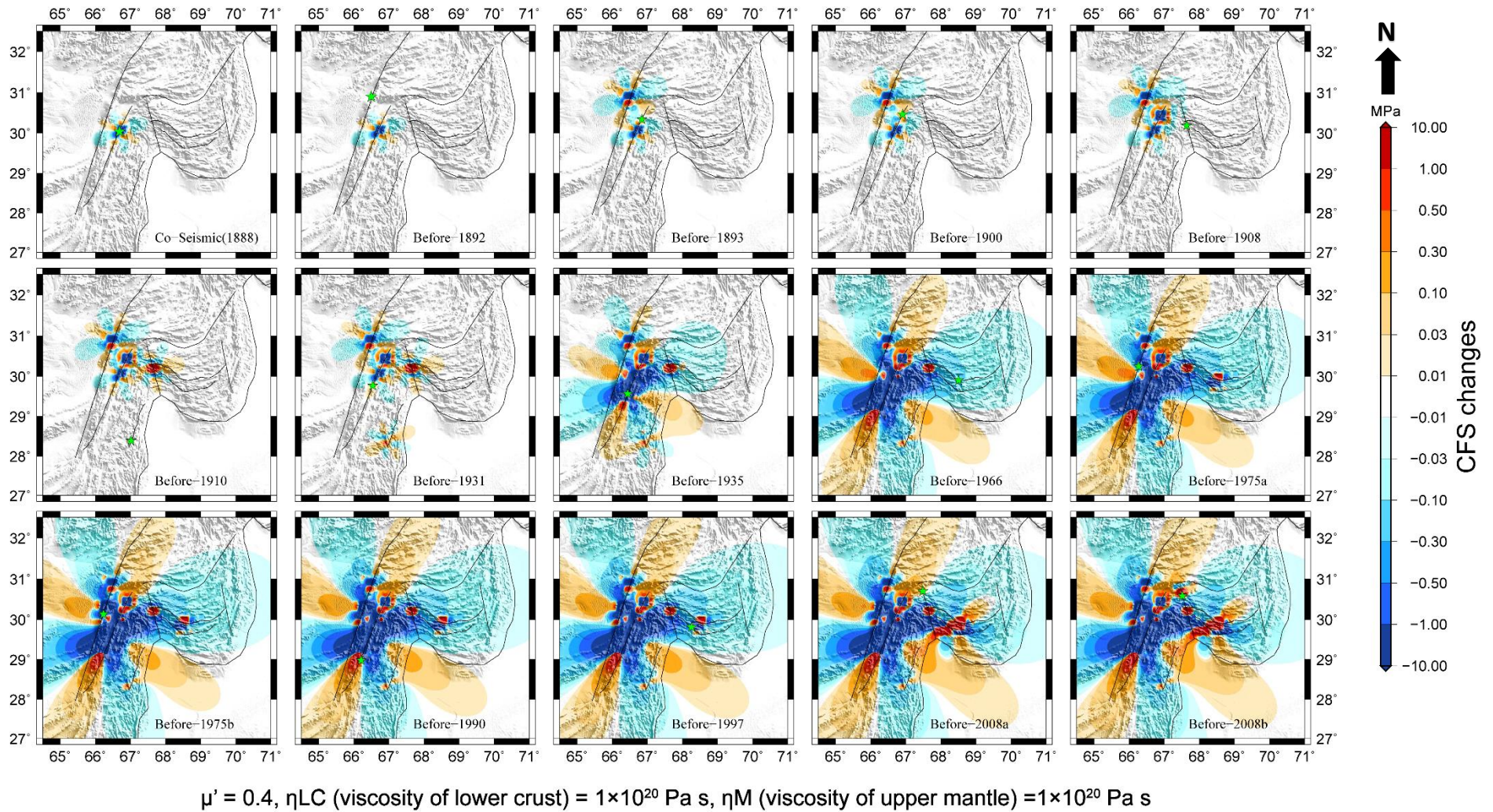
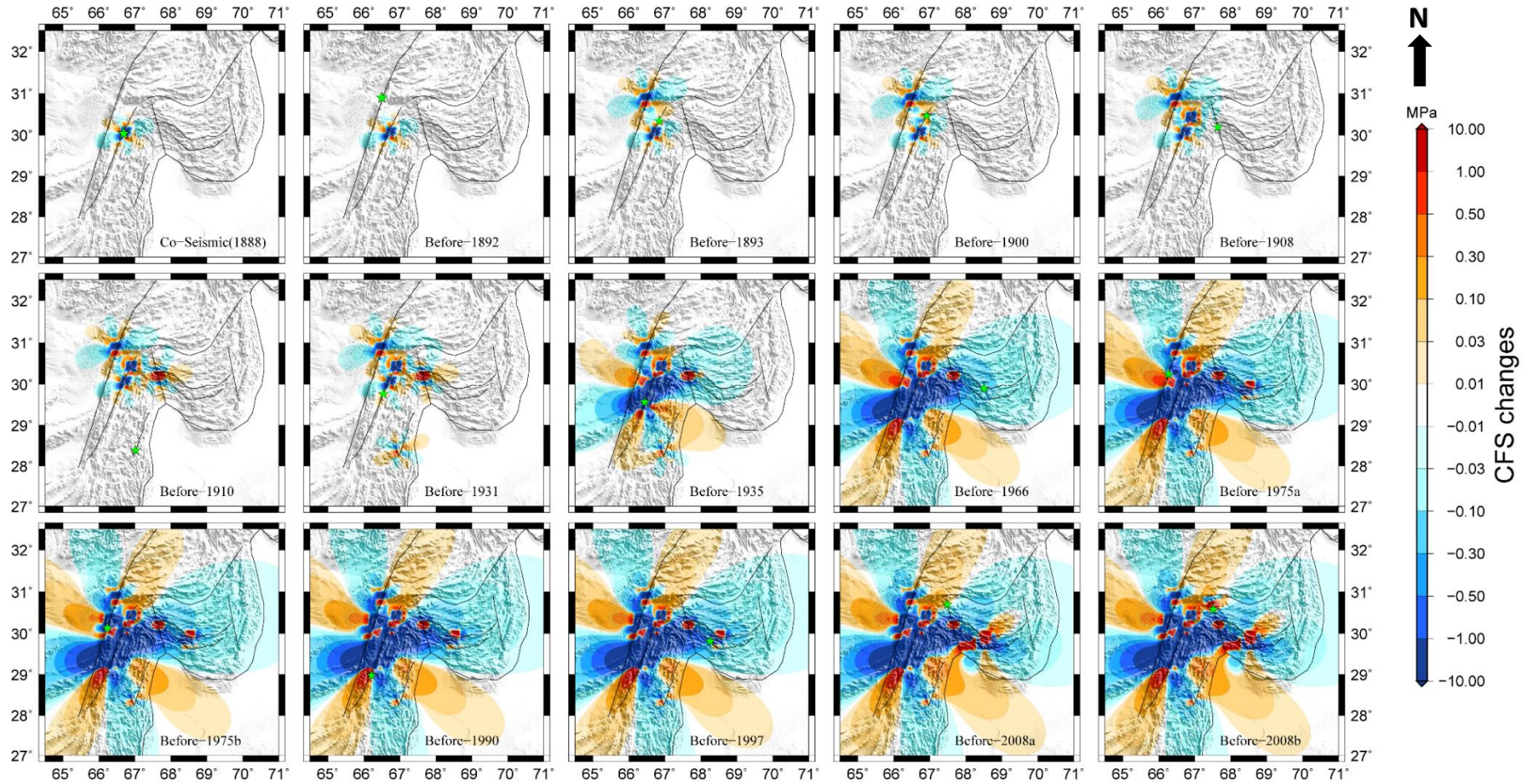


Figure 5.15. (a-o) The Δ CFS evolution at the 10km depth since 1888. Active faults in the study area are indicated by black lines. The Green star indicates the portion of next earthquake rupture. The Δ CFS is depicted in each snapshot series just before the subsequent earthquake. The increased and decreased Δ CFS are represented by warm and cool tones.



$$\mu' = 0.6, \eta_{LC} (\text{viscosity of lower crust}) = 1 \times 10^{20} \text{ Pa s}, \eta_M (\text{viscosity of upper mantle}) = 1 \times 10^{20} \text{ Pa s}$$

Figure 5.16. (a-o) The Δ CFS evolution at the 10km depth since 1888. Active faults in the study area are indicated by black lines. The Green star indicates the portion of next earthquake rupture. The Δ CFS is depicted in each snapshot series just before the subsequent earthquake. The increased and decreased Δ CFS are represented by warm and cool tone.

The numerical results show that choosing a lower viscosity resulted in a quicker relaxation, eventually a rapid stress accumulation and vice versa. It is because a lower viscosity value accelerates the post-seismic viscoelastic relaxation process. The co-seismic stress change that occurs after the co-seismic elastic deformation causes a viscoelastic flow (Freed et al., 2005). The viscosity of the lower crust primarily controls the speed of stress transfer; the lower the viscosity, the faster the transfer speed and vice versa. The results of our tests with varied viscosity values revealed that while the magnitude of ΔCFS varies slightly, it has no effect on the ΔCFS pattern and the triggering relationship among the sequence over the timescale of this study (Verdecchia and Carena, 2015).

Based on the findings, we deduced that eight out of the fifteen earthquakes are potentially triggered by the preceding events. The 1892 earthquake (Mw 6.8), which occurred on the northern segment of the Chaman fault had a little impact on the 1935 event which occurred on the Ghazaband fault. The 1935 earthquake induced large positive stress at either end of its ruptured portion, triggering the 1975 earthquake on the Chaman fault in the northern stress-positive lobe. The 1975 earthquake occurred in the southern positive ΔCFS lobe caused by the 1892 earthquake, but the 1935 earthquake narrowed that positive lobe and formed a stress shadow zone at both ends of the 1975 earthquake. As a result, we concluded that the stress shadow induced by the 1935 event retarded the failure on the Chaman fault until 1975. Also It is further deduced that the 1935 event was primarily responsible for the stress orientation in the Chaman fault system. The 1990 earthquake occurred in the southern zone of positive stress at the rupture segment of the 1935 event. The 2008 Ziarat doublet earthquakes occurred on the northern- stress positive lobe of the 1935 event's rupture segment. The 2008 doublet is triggered by preceding events. The epicenter of 2008b earthquake is in positive CFS zone generated by both preceding events and 2008a event.

The northern segment of Chaman fault, southern segment of the Ghazaband fault and the northwestern segment of Urghargai fault demonstrates a high positive ΔCFS (red lobes) in the stress maps which indicates that, these segments are vulnerable to seismic hazards (Fig 5.17).

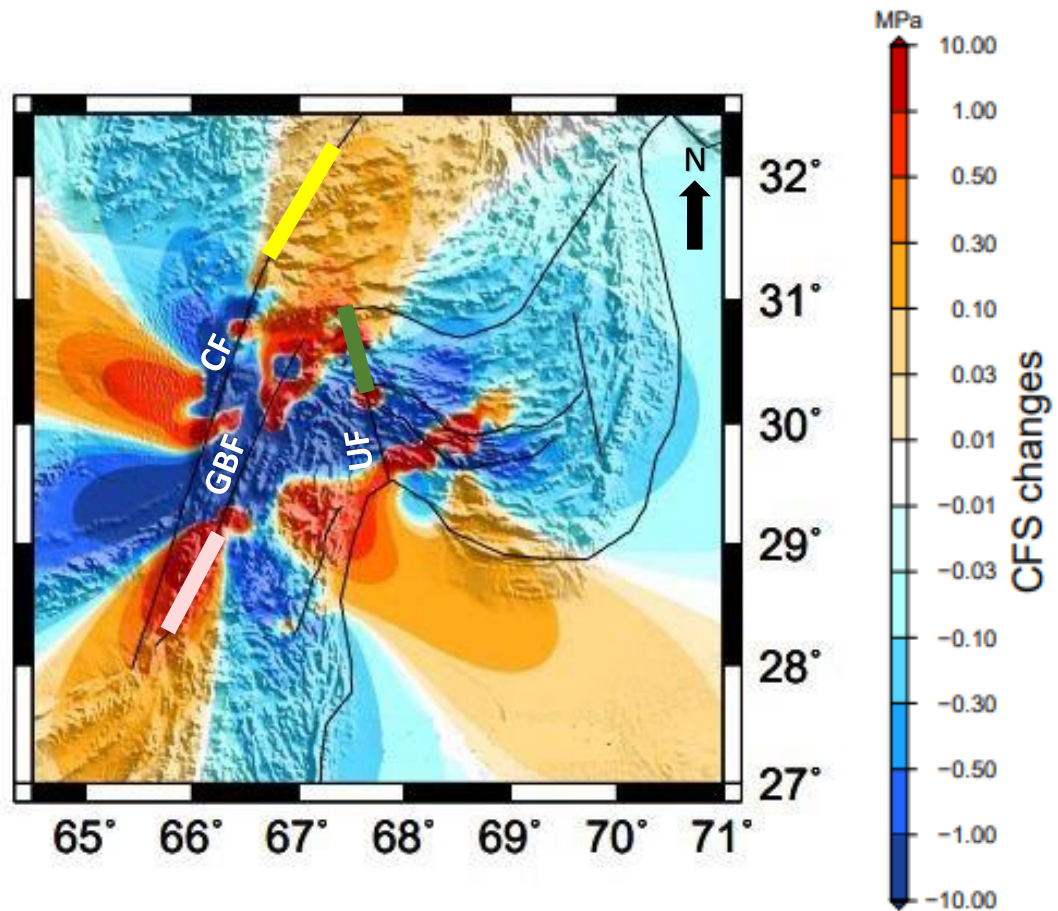


Figure 5.17 Hazard map of study area. Yellow thick line indicates northern segment of Chaman fault (CF), Pink thick line indicates southern segment of Ghazaband fault (GBF) and thick green line indicates northwestern segment of Urghargai fault (UF) with high Δ CFS values respectively.

CONCLUSIONS

A sequence of earthquakes comprised of 15 events is chosen after rigorous investigation of online and published earthquake catalogues. Following that, we used PSGRN/PSCMP to calculate co- and post-seismic stress transfer. We also performed several simulations with varying values of the co-efficient of friction and the lower crust and upper mantle viscosities for the robustness of our numerical results.

1. The Δ CFS value for 1893,1900,1931,1935,1975,1990, and 2008 is higher than the earthquake triggering value, 0.01 MPa, by mutual contribution of co- and post-seismic stress transfer. It indicates a significant contribution of Δ CFS to advances the occurrence of impending earthquakes.
2. Moreover, we also infer that the co-stress is not the only major driving force that caused the occurrence of subsequent events. But the post-seismic viscoelastic relaxation process plays more significant role in the stress transfer and accumulation followed by the major earthquakes.
3. Despite using different values for the lower crust and upper mantle viscosities and co-efficient of friction, our results demonstrated a significant interaction between earthquakes and faults in region of interest.
4. The northern segment of Chaman fault, southern segment of the Ghazaband fault and the northwestern segment of Urghargai fault demonstrates a high positive Δ CFS (red lobes) in the above mentioned stress map which indicates that, these segments are vulnerable to seismic hazards.
5. The seismic hazard maps emphasized that some regions needed to be investigated more extensively due to hazard levels expected there. This research work is an attempt to increase our understanding concerning the earthquake triggering and fault interaction in the region of interest. For future work, an improved CFS maps related to earthquake triggering may be produced by incorporating definite lithospheric dynamics which requires instrumental data investigations for the area being studied.

REFERENCES

- Ambraseys, N., & Douglas, J. (2004). Magnitude calibration of north Indian earthquakes. *Geophysical Journal International*, 159(1), 165-206.
- Abdel-Gawad, M. (1971). Wrench movements in the Baluchistan arc and relation to Himalayan-Indian Ocean tectonics. *Geological Society of America Bulletin*, 82(5), 1235-1250.
- Ahmed, Z. A., & Abbas, S. (1979). Ophiolites in Pakistan: an introduction *Geodynamics of Pakistan* (pp. 181-192): Geol. Surv. Pakistan Quetta.
- Allemann, F. (1979). Time of emplacement of the Zhob Valley ophiolite and Bela ophiolites, Baluchistan. *Geodynamics of Pakista*, edited by A. Farah and KA De Jong, 215-242.
- Ahmad, S. (2009). Seismicity in Pakistan during 2008 and Local Site Response in Muzaffarabad and Islamabad, Pakistan (Master's thesis, The University of Bergen).
- Ambraseys, N. & Bilham, R., 2003. Earthquakes and associated deformation in northern Baluchistan, *Bull. seism. Soc. Am.*, 93, 1573–1605.
- Aki K, Richards PG (2002) *Quantitative Seismology* 2nd edn. University Science Books, California.
- Blanford, W. T. (1883). Geological notes on the hills in the neighborhood of the Sind and Punjab Frontier between Quetta and Dera Ghazi Khan. *Memoirs of the geological survey of India*, 20, 105-240.
- Bannert, D. & Raza, H. A., 1992. The segmentation of the Indo-Pakistan Plate. *Pak. J. Hydrocarbon Res.*, 4(2): 5-18.
- Bender, F., & Raza, H. A. (1995). *Geology of Pakistan*.
- Bernard, M., Shen-Tu, B., Holt, W.E. & Davis, D.M. 2000. Kinematics of active deformation in the Sulaiman lobe and range, Pakistan, *J. geophys. Res.*, 105(6), 13 253–13 279.

- Chandra, U. (1978). Seismicity, earthquake mechanisms and tectonics along the Himalayan mountain range and vicinity. *Physics of the Earth and Planetary Interiors*, 16(2), 109-131.
- Davies, L. M. (1940). Geographical Changes in North-West India during late Cretaceous and early Tertiary times. *Proc. Sixth Pacific Sci. Congr.(1939), II*, 483-501.
- DeMets, C., R. G. Gordon, D. F. Argus, and S. Stein, Effects of recent revisions to the geomagnetic reversal time scale on estimates of current plate motions, *Geophys. Res. Lett.*, 21, 2191-2194, 1994.
- Eames, F. (1952). A contribution to the study of the Eocene in western Pakistan and western India C. The description of the Scaphopoda and Gastropoda from Standard sections in the Rakhi Nala and Zinda Pir areas of the western Punjab and in the Kohat district. *Philosophical Transactions of the Royal Society of London. Series B, Biological Sciences*, 1-168.
- Freed, A. M. (2005). EARTHQUAKE TRIGGERING BY STATIC, DYNAMIC, AND POSTSEISMIC STRESS TRANSFER. *Annual Review of Earth and Planetary Sciences*, 33(1), 335-367. doi: 10.1146/annurev.earth.33.092203.122505.
- Farah, A., Lawrence, R. D., and Dejong, K. A., 1984, An overview of the tectonics of Pakistan, in *Marine Geology and Oceanography of Arabian Sea and Coastal Pakistan*, eds., B.U.Haq and J.D.Milliman, Van Nostrand Reinhold, p.161-176.
- Gansser, A. (1979). Reconnaissance visit to the ophiolites in Baluchistan and the Himalaya. *Geodynamics of Pakistan*, 193-213.
- Gansser, A., 1981. Zagia, Hindukush, Himalaya, geodynamic evolution (ed. H. K., Gupta & F. M. Delaney), *Am. Geophysics. Union, Geodynamic Series.*, Vol 3, 111- 121.
- Griesbach, C. L., 1893. On the geology of the country between Chappar Rift and Harnai in Baluchistan. *Geol. Surv. India, Rec.* 26: 113-147.
- Global CMT Catalogue Search: available at web page :
- <http://www.globalcmt.org/CMTsearch.html>**.
- Hemphill, W. R., & Kidwai, A. H. (1973). Stratigraphy of the Bannu and Dera Ismail Khan areas, Pakistan.

- IAEA, "Evaluation of Seismic Hazards for Nuclear Installations," IAEA (International Atomic Energy Agency) Safety Guide No. NS-G-3.3, November, 2008.
- Jadoon, I. A. K. (1991). Thin-skinned tectonics on continent/ocean transitional crust, Sulaiman Range, Pakistan.
- Jones, A. (1961). Reconnaissance geology of part of West Pakistan (Ed.), A Colombo Plan Cooperative Project, Hunting Survey Corporation: Maracle Press, Toronto.
- Jadoon, I., Lillie, R., Humayon, M., Lawrence, R., Ali, S., & Cheema, A. (1989). Mechanism of deformation and the nature of the crust underneath the Himalayan foreland fold-and-thrust belts in Pakistan. *EOS. Transaction, American Geophysical Union*, 70, 1372-1373.
- Jadoon, I., Lawrence, R., & Lillie, R. (1992). Balanced and retrodeformed geological cross-section from the frontal Sulaiman Lobe, Pakistan: Duplex development in thick strata along the western margin of the Indian Plate *Thrust Tectonics* (pp. 343-356): Springer.
- Jadoon, I., Frisch, W., Kemal, A., & Jaswal, T. (1997). Thrust geometries and kinematics in the Himalayan foreland (North Potwar deformed zone), North Pakistan. *Geologische Rundschau*, 86(1), 120-131.
- Jadoon, I. A., & Khurshid, A. (1996). Gravity and tectonic model across the Sulaiman fold belt and the Chaman fault zone in western Pakistan and eastern Afghanistan. *Tectonophysics*, 254(1-2), 89-109.
- Jackson, J., J. Haines, and W. Holt, The accommodation of Arabian-Eurasian plate motion in Iran, *J. Geophys. Res.*, 100, 15,205-15,219, 1995.
- Jadoon, I. A. K., Lillie, R. J. & Lawrence, R. D., 1993. Balanced structural cross-section of the sulaiman Lobe, Pakistan: Evolution, geometry, shortening and hydrocarbon prospects of a thrust system at the western terminus of the Indian Plate. *Pak. J. Hydrocarbon Res.*, 5 (1 & 2); 15-36
- Jan, M. Q. (2010). Geoseismological study of the Ziarat (Baluchistan) earthquake (doublet?) of 28 October 2008. *Current Science*, 50-57.
- Kirsty Reynolds, Alex Copley, Ekbal Hussain, Evolution and dynamics of a fold-thrust belt: the Sulaiman Range of Pakistan, *Geophysical Journal International*, Volume 201, Issue 2, May, 2015, Pages 683–710.

- Kazmi, A. (1979). A report on active fault systems in Pakistan. *Geodynamics of Pakistan, Geological Survey of Pakistan, Spec. Issue*, 285-289.
- Kadri, I.B. 1995. Petroleum Geology of Pakistan. Pakistan Petroleum Limited, Karachi. 275.
- Kazmi, A. H., 1979a. Active fault systems in Pakistan. In: Farah, A. & DeJong, K. A. (eds.) geodynamics of Pakistan. Geol. Surv. Pak., Quetta, 285-294.
- Kazmi, A. H. & Rana, R.A. 1982. Tectonic map of Pakistan. Geol. Surv. Pak., Quetta. Scale 1:2,000,000.
- King GCP, Stein RS, Lin J (1994) Static stress changes and the triggering of earthquakes. *Bull Seismol Soc Am* 84:935–953.
- Lillie, R., Lawrence, R., Humayon, M., & Jadoon, I. (1989). The Sulaiman thrust lobe of Pakistan: Early stage underthrusting of the Mesozoic rifted margin of the Indian subcontinent. *Geological Society of America*.
- Lawrence, R., Yeats, R., Khan, S., Farah, A., & DeJong, K. (1981). Thrust and strike slip fault interaction along the Chaman transform zone, Pakistan. *Geological Society, London, Special Publications*, 9(1), 363-370.
- Malik, Z., Kemal, A., Malik, A. M., & Bodenhausen, J. (1988). *Petroleum potential and prospects in Pakistan*. Paper presented at the International Symposium on Petroleum for the Future.
- Mahdi, S. K. (2010). Some Seismological Characteristics of Mw 6.5 Pishin-Ziarat October 29, 2008 Double Earthquake.
- Molnar, P., Fitch, T. J., & Wu, F. T. (1973). Fault plane solutions of shallow earthquakes and contemporary tectonics in Asia. *Earth and Planetary Science Letters*, 19(2), 101-112.
- Oldham, R. (1890). *Report on the geology and economic resources of the country adjoining the Sind-Pishin railway between Sharigh and Spintangi, and of the country between it and Khattan*.
- Olson, T. M. (1982). *Sedimentary tectonics of the Jalipur sequence, northwest Himalaya, Pakistan* (Doctoral dissertation, Dartmouth College).
- Pinfold, E. (1939). The Dunghan Limestone and the Cretaceous-Eocene unconformity in North-West India. *Rec. Geol. Surv. India*, 74, 189.

- Quittmeyer, R., & Jacob, K. (1979). Historical and modern seismicity of Pakistan, Afghanistan, northwestern India, and southeastern Iran. *Bulletin of the Seismological Society of America*, 69(3), 773-823.
- Quittmeyer, R. C., & Kafka, A. L. (1984). Constraints on plate motions in southern Pakistan and the northern Arabian Sea from the focal mechanisms of small earthquakes. *Journal of Geophysical Research: Solid Earth*, 89(B4), 2444-2458.
- Qayyum, M., Niem, A. R., & Lawrence, R. D. (1996). Newly discovered Paleogene deltaic sequence in Katawaz basin, Pakistan, and its tectonic implications. *Geology*, 24(9), 835-838.
- Rowlands, D. (1978). The structure and seismicity of a portion of the southern Sulaiman Range, Pakistan. *Tectonophysics*, 51(1-2), 41-56.
- Rafi, Z., & Ahmed, N. Seismotectonic analysis of Ziarat, Baluchistan Earthquake of 29 th OCT, 2008.
- Raza HA, Ahmed R, Alam S, Ali SM (1989b) Petroleum zones of Pakistan. *Pak J Hydrocarb Res* 1(2) : 1—20
- Rehman, S. U., Lindholm, C., Ahmed, N., & Rafi, Z. (2014). Probabilistic seismic hazard analysis for the city of Quetta, Pakistan. *Acta Geophysica*, 62(4), 737-761
- Rowlands, D. (1978). The structure and seismicity of a portion of the southern Sulaiman Range, Pakistan. *Tectonophysics*, 51(1-2), 41-56.
- Sultan M (2015) Seismic Hazard Analysis of Pakistan. *J Geol Geosci* 4: 190.
- Sarwar, G., & De Jong, K. (1979). *Geodynamics of Pakistan*.
- Scholz CH (1990) *The Mechanics of earthquakes and faulting*. Cambridge Univ Press, New York, p 439.
- Verdecchia, A., & Carena, S. (2015). One hundred and fifty years of Coulomb stress history along the California-Nevada border, USA. *Tectonics*, 34(2), 213-231.
- Wang, Z. (2011). Seismic hazard assessment: issues and alternatives. *Pure and Applied Geophysics*, 168(1-2), 11-25.
- Wells DL, Coppersmith KJ (1994) New empirical relationships among magnitude, rupture length, rupture width, rupture area, and surface displacement. *Bull Seism Soc Am* 84:974–1002.

- Wang R, Lorenzo-Martín F, Roth F (2006) PSGRN/PSCMP—a new code for calculating co- and post-seismic deformation, geoid and gravity changes based on the viscoelastic-gravitational dislocation theory. *Comput Geosci* 32:527–541.
- Xiong X, Shan B, Zhou YM, Wei SJ, Li YD, Wang RJ, Zheng Y (2017) Coulomb stress transfer and accumulation on the Sagaing Fault, Myanmar, over the past 110 years and its implications for seismic hazard. *Geophys Res Lett.* <https://doi.org/10.1002/2017gl072770>
- Yadav, R.B.S., Gahalaut, V.K., Sumer, C. & Bin, S., 2012. Tectonic implications and seismicity triggering during the 2008 Baluchistan, Pakistan earthquake sequence, *J. Asian Earth Sci.*, 45, 167–178.

APPENDIX I

No	DATE			TIME			EPICENTRE		h (km)	Mw	Strike/ Dip/Rake (m)	Length/ Width(Km)
	yy	mm	dd	hh	m	ss	lat(N)	long (E)				
1	1888	10	28	0	0	0	30.2	67	20	6.3	20/90/10	167/20
2	1888	12	28	0	0	0	30.2	67	20	7	20/90/10	167/20
3	1892	12	20	0	0	0	31	66	20	6	20/90/10	167/20
4	1892	12	20	0	0	0	30.9	66.5	20	6.5	20/90/10	167/20
5	1893	2	0	0	0	0	30.2	67	1.8	6.8	20/80/9	7.7/8
6	1893	2	13	0	0	0	30.2	67	1.7	6	20/80/9	7.7/8
7	1900	0	0	0	0	0	30.42	67	1.7	6.1	20/80/9	7.7/8
8	1902	0	0	0	0	0	30.63	66.75	15	5.5	20/90/10	167/20
9	1908	1	12	0	0	0	30.2	67.7	17	5.75	304/73/171	21/21
10	1908	3	5	0	0	0	30.2	67.7	1.7	6.36	304/73/171	-
11	1910	8	17	0	0	0	28.4	67	28	6.26	278/78/-176	12/7
12	1913	3	27	0	0	0	29.5	67.5	17.2	5.78	304/73/171	21/21
13	1914	5	21	0	0	0	31.95	69.96	29	5.82	180/18/71	-
14	1914	11	4	0	0	0	32	70	29	5.84	180/18/71	-
15	1918	11	29	0	0	0	32.7	67.7	20	6.17	20/90/10	167/20
16	1927	1	30	0	0	0	30.18	70.32	11	5.69	225/18.5/89.7	7.7/8
17	1928	12	14	0	0	0	28.81	68.08	5.5	5.79	237/32/111	151.8/0
18	1928	12	12	0	0	0	29.68	69.12	5.5	5.5	237/32/111	151.8/0
19	1931	8	25	3	6	0	31.49	66.52	1.7	5.7	20/80/9	7.7/8
20	1931	8	27	0	0	0	29.9	67.2	1.7	7.24	20/80/9	7.7/8
21	1931	10	3	0	0	0	29.8	67.3	17	5.65	304/73/171	21/21
22	1931	8	28	0	0	0	28.82	67.39	17	5.73	304/73/171	21/21
23	1931	8	25	0	0	0	30.2	67.7	17	5.54	304/73/171	21/21
24	1931	9	6	0	0	0	29.72	67.85	17	5.65	304/73/171	21/21
25	1935	6	2	9	16	0	30.14	66.93	13	6.1	20/80/9	7.7/20
26	1935	5	30	0	0	0	28.87	66.4	20	7.4	33/68/124	167/20
27	1935	5	15	0	0	0	28.4	67.5		6.01	33/68/124	-
28	1935	10	28	0	0	0	31.3	69.3	29	5.75	180/18/71	-
29	1938	12	1	0	0	0	30.43	68.53	29	5.65	180/18/71	-
30	1941	9	29	0	0	0	30.19	67.09		5.67	20/80/9	7.7/8
31	1952	12	25	0	0	0	29.25	70	15	5.96	225/18.5/89.7	7.7/8
32	1952	9	15	11	28	20	30.58	70.01	15	5.71	243/39/92	7.7/0
33	1955	2	9	0	0	0	30.5	67	0	5.8	20/80/9	7.7/0
34	1955	2	18	22	48	0	30.2	67	33	5.8	20/80/9	7.7/8
35	1956	1	11	0	0	0	29.99	69.55	5.5	5.69	243/39/92	7.7/0
36	1960	10	3	0	0	0	29.76	68.25	5.5	5.63	243/39/92	-

37	1966	2	7	23	6	34	29.8	69.5	9	5.8	237.6/46.7/107.9	-
38	1966	8	1	21	3	1	30.05	68.63	3	6.2	204.8/42.7/62.6	-
39	1966	1	24	7	23	10	29.93	69.69	8	5.5	223.3/37.3/96.6	-
40	1966	2	13	0	0	0	29.95	69.67	8	5.5	223.3/37.3/96.6	-
41	1971	1	8	0	0	0	29.28	69.13	8	5.5	270/10/110	-
42	1973	1	20	0	0	0	29.42	68.55	8	5.7	223.3/37.3/96.6	-
43	1973	11	4	5	10	8	30.7	66.3	33	5.5	20/90/10	167/20
44	1975	10	3	17	31	36	30.44	66.41	23.7	5.6	20/90/10	167/20
45	1975	10	3	5	14	24	30.24	66.28	11	6.8	20/80/0.34	18.2/9.9
46	1975	10	3	0	0	0	30.24	66.29	20	6.6	20/90/10	167/20
47	1975	3	22	0	0	0	29.97	69.12	7	5.5	85/29/60	-
48	1977	7	13				29.88	67.45	15	5.5	109/75/166	-
49	1978	5	6	11	16	7	29.84	66.21	33	5.7	101/79/-179	167/20
50	1985	5	6	0	0	0	30.85	70.27	11	5.8	225/18.5/89.7	-
51	1988	3	19	0	0	0	30.06	67.94	15	5.7	142/60/-7	-
52	1990	4	27	5	29	39	30	65.3	0	5.7	101/79/-179	-
53	1990	3	4	0	0	0	28.66	66.16	28	6.2	278/78/-176	12/7
54	1992	2	5	23	10	50	31.42	66.92	15	5.5	299/87/-177	167/20
55	1992	2	5	11	10	50	31.42	66.92	15	5.5	20/90/10	167/20
56	1992	2	5	15	7	12	31.43	66.83	17	5.7	20/90/10	167/20
57	1992	2	5	23	10	49	31.44	66.87	17.9	5.5	20/90/10	167/20
58	1992	8	28	0	50	49	29.2	66.8	15	5.6	118/67/179	-
59	1993	11	16	15	52	47	30.54	66.88	33	5.6	114/77/179	-
60	1995	6	11	0	0	0	32.58	69.69	29	5.65	180/18/171	-
61	1997	2	27	21	30	54	31	66	15.3	7.1	298/15/122	67/23
62	1997	8	24	0	0	16	30.12	67.96	16	5.6	262/16/77	-
63	1997	3	20	8	50	45	30.1	68.01	15	5.91	76/7/-91	-
64	1997	3	4	0	0	0	29.42	68.79	15	5.7	58/74/11	-
65	1999	6	26	21	54	29	31	66.7	5.5	5.5	243/39/92	151.8/0
66	1999	7	12	0	0	0	29.99	69.46	5	5.6	28/35/82	151.8/0
67	1999	7	28	0	0	0	29.87	69.47	5.5	5.5	237/32/111	151.8/0
68	2008	10	28	23	10	2	30.656	67.361	17.2	6.4	304/73/171	21/21
69	2008	10	29	11	32	49	30.6	67.46	12	6.4	324/68/-178	21/19.5
70	2008	12	9	0	0	0	30.433	67.414	22	5.5	62/65/-5	-
71	2008	12	9	22	52	40	30.4	67.4	12	5.7	330/87/173	21/21
72	2016	5	13	7	1	8.4	30.69	66.57	22.1	5.6	111/70/0	20/0

APPENDIX II

Earthquake parameters calculation using empirical relation used in the study.

	YY-MM-DD	Lat (N)	Long (E)	Mw	Length/Width/Average slip (km/km/m)	Fault Geometry Strike/Dip/Rake	Fault type
1	1888-10-28	30.2	67	6.3	12.9/ 8.7/0.22	20/90/10	Strike slip
2	1888-12-28	30.2	67	7	42.7/13.5/0.95	20/90/10	Strike slip
3	1892-12-20	31	66	6	7.8/7.2/0.12	20/90/10	Strike slip
4	1892-12-20	30.9	66.5	6.5	18.2/9.9/0.34	20/90/10	Strike slip
5	1893-02-0	30.2	67	6.8	30.3/11.9/0.63	20/80/9	Strike slip
6	1893-02-13	30.2	67	6	7.8/7.2/0.12	20/80/9	Strike slip
7	1900-0-0	30.42	67	6.1	9.2/7.7/0.15	20/80/9	Strike slip
8	1902-0-0	30.63	66.75	5.5	3.3/5.3/0.04	20/90/10	Strike slip
9	1908-01-12	30.2	67.7	5.75	5.1/6.2/0.07	304/73/171	Strike slip
10	1908-03-5	30.2	67.7	6.36	14.3/9.1/0.25	304/73/171	Strike slip
11	1910-08-17	28.4	67	6.26	12.1/8.5/0.21	278/78/-176	Strike slip
12	1913-03-27	29.5	67.5	5.78	5.3/6.3/0.08	304/73/171	Strike slip
13	1914-05-21	31.95	69.96	5.82	6.4/6/0.53	180/18/71	Thrust
14	1914-11-4	32	70	5.84	6.6/6.1/0.53	180/18/71	Thrust
15	1918-11-29	32.7	67.7	6.17	10.4/8.1/0.17	20/90/10	Strike slip
16	1927-01-30	30.18	70.32	5.69	5.3/5.3/0.52	225/18.5/89.7	Thrust
17	1928-12-14	28.81	68.08	5.79	6.1/5.8/0.53	237/32/111	Thrust
18	1928-12-12	29.68	69.12	5.5	4/4.4/0.5	237/32/111	Thrust
19	1931-08-25	31.49	66.52	5.54	3.5/5.4/0.05	20/80/9	Thrust
20	1931-08-27	29.9	67.2	7.24	64.2/15.7/1.57	20/80/9	Strike slip
21	1931-10-3	29.8	67.3	5.65	4.3/5.8/0.06	304/73/171	Strike slip
22	1931-08-28	28.82	67.39	5.73	4.9/6.1/0.07	304/73/171	Strike slip
23	1931-08-25	30.2	67.7	5.54	3.5/5.4/0.05	304/73/171	Strike slip
24	1931-09-06	29.72	67.85	5.65	4.3/5.8/0.06	304/73/171	Strike slip
25	1935-06-02	30.14	66.93	6.1	9.2/7.7/0.15	20/80/9	Strike slip
26	1935-05-30	28.87	66.4	7.4	84.3/17.3/2.19	33/68/124	Strike slip
27	1935-05-15	28.4	67.5	6.01	7.9/7.3/0.12	33/68/124	Strike slip
28	1935-10-28	31.3	69.3	5.75	5.8/5.6/0.52	180/18/71	Thrust
29	1938-12-01	30.43	68.53	5.65	5/5.1/0.52	180/18/71	Thrust
30	1941-09-29	30.19	67.09	5.67	4.4/5.9/0.06	20/80/9	Strike slip
31	1952-12-25	29.25	70	5.96	7.8/6.8/0.55	225/18.5/89.7	Thrust
32	1952-09-15	30.58	70.01	5.71	4.7/6/0.07	243/39/92	Strike slip
33	1955-02-09	30.5	67	5.8	5.5/6.4/0.08	20/80/9	Strike slip
34	1955-02-18	30.2	67	5.8	5.5/6.4/0.08	20/80/9	Strike slip
35	1956-01-11	29.99	69.55	5.69	5.3/5.3/0.52	243/39/92	Thrust
36	1960-10-03	29.76	68.25	5.63	4.9/5/0.51	243/39/92	Thrust
37	1966-02-07	29.8	69.5	5.8	5.5/6.4/0.08	237.6/46.7/107.9	Strike slip

38	1966-08-01	30.05	68.63	6.2	11.1/8.6/0.57	204.8/42.7/62.6	Thrust
39	1966-01-24	29.93	69.69	5.5	4/4.4/0.5	223.3/37.3/96.6	Thrust
40	1966-02-13	29.95	69.67	5.5	4/4.4/0.5	223.3/37.3/96.6	Thrust
41	1971-01-08	29.28	69.13	5.5	4/4.4/0.5	270/10/110	Thrust
42	1973-01-20	29.42	68.55	5.7	5.4/5.3/0.52	223.3/37.3/96.6	Thrust
43	1973-11-04	30.7	66.3	5.5	3.3/5.3/0.04	20/90/10	Strike slip
44	1975-10-03	30.44	66.41	5.6	3.9/5.6/0.05	20/90/10	Strike slip
45	1975-10-03	30.24	66.28	6.8	30.3/11.9/0.63	20/80/0.34	Strike slip
46	1975-10-03	30.24	66.29	6.6	21.6/10.5/0.42	20/90/10	Strike slip
47	1975-03-22	29.97	69.12	5.5	3.3/5.3/0.04	85/29/60	Thrust
48	1977-07-13	29.88	67.45	5.5	3.3/5.3/0.04	109/75/166	Strike slip
49	1978-05-06	29.84	66.21	5.7	4.7/6/0.06	101/79/-179	Strike slip
50	1985-05-06	30.85	70.27	5.8	6.2/5.9/0.53	225/18.5/89.7	Thrust
51	1988-03-19	30.06	67.94	5.7	4.7/6/0.06	142/60/-7	Strike slip
52	1990-04-27	30	65.3	5.7	4.7/6/6	101/79/-179	Strike slip
53	1990-03-04	28.66	66.16	6.2	7.8/7.2/0.12	278/78/-176	Strike slip
54	1992-02-05	31.42	66.92	5.5	3.3/5.3/0.04	299/87/-177	Strike slip
55	1992-02-05	31.42	66.92	5.5	3.3/5.3/0.04	20/90/10	Strike slip
56	1992-02-05	31.43	66.83	5.7	4.7/6/0.06	20/90/10	Strike slip
57	1992-02-05	31.44	66.87	5.5	3.3/5.3/0.04	20/90/10	Strike slip
58	1992-08-28	29.2	66.8	5.6	3.9/5.6/0.05	118/67/179	Strike slip
59	1993-11-16	30.54	66.88	5.6	3.9/5.6/0.05	114/77/179	Strike slip
60	1995-06-11	32.58	69.69	5.65	5/5.1/0.52	180/18/171	Thrust
61	1997-02-27	31	66	7.1	50.6/14.4/1.17	298/15/122	Strike slip
62	1997-08-24	30.12	67.96	5.6	4.7/4.9/0.04	262/16/77	Thrust
63	1997-03-20	30.1	68.01	5.91	7.3/6.5/0.54	76/7/-91	Thrust
64	1997-03-04	29.42	68.79	5.7	5.4/5.3/0.52	58/74/11	Thrust
65	1999-06-26	31	66.7	5.5	4/4.4/0.5	243/39/92	Thrust
66	1999-07-12	29.99	69.46	5.6	4.7/4.9/0.51	28/35/82	Thrust
67	1999-07-28	29.87	69.47	5.5	4/4.4/0.5	237/32/111	Thrust
68	2008-10-28	30.656	67.361	6.4	15.3/9.3/0.28	304/73/171	Strike slip
69	2008-10-29	30.6	67.46	6.4	15.3/9.3/0.28	324/68/-178	Strike slip
70	2008-12-09	30.433	67.414	5.5	3.3/5.3/0.04	62/65/-5	Strike slip
71	2008-12-09	30.4	67.4	5.7	4.7/6/0.06	330/87/173	Strike slip
72	2016-05-13	30.69	66.57	5.6	3.3/5.3/0.04	111/70/0	Strike slip

hazard analysis

ORIGINALITY REPORT

14%

SIMILARITY INDEX

8%

INTERNET SOURCES

10%

PUBLICATIONS

2%

STUDENT PAPERS

PRIMARY SOURCES

1

link.springer.com

Internet Source

2%

2

Bin Shan, Xiong Xiong, Yong Zheng, BiKai Jin, ChengLi Liu, ZhuJun Xie, HouTze Hsu. "Stress changes on major faults caused by 2013 Lushan earthquake and its relationship with 2008 Wenchuan earthquake", Science China Earth Sciences, 2013

Publication

2%

3

Submitted to Higher Education Commission Pakistan

Student Paper

1%

4

Shan, B.. "The co-seismic Coulomb stress change and expected seismicity rate caused by 14 April 2010 Ms=7.1 Yushu, China, earthquake", Tectonophysics, 20111004

Publication

1%

5

Bin Shan, Xiong Xiong, Rongjiang Wang, Yong Zheng, Song Yang. "Coulomb stress evolution along Xianshuihe–Xiaojiang Fault System since 1713 and its interaction with Wenchuan

1%

earthquake, May 12, 2008", Earth and Planetary Science Letters, 2013

Publication

6	www.scribd.com Internet Source	1 %
7	www.ppisonline.com Internet Source	1 %
8	academic.oup.com Internet Source	1 %
9	Giuseppe Pezzo, John Peter Merryman Boncori, Simone Atzori, Andrea Antonioli, Stefano Salvi. "Deformation of the western Indian Plate boundary: insights from differential and multi-aperture InSAR data inversion for the 2008 Baluchistan (Western Pakistan) seismic sequence", Geophysical Journal International, 2014 Publication	<1 %
10	en.wikipedia.org Internet Source	<1 %
11	gitext.gfz-potsdam.de Internet Source	<1 %
12	ulster.pure.elsevier.com Internet Source	<1 %
13	Muhammad Shahid Riaz, Shan Bin, Shahid Naeem, Wang Kai, Zujun Xie, Syed Mushhad	<1 %

M. Gilani, Umer Ashraf. "Over 100 years of faults interaction, stress accumulation, and creeping implications, on Chaman Fault System, Pakistan", International Journal of Earth Sciences, 2019

Publication

14

www.scialert.net

Internet Source

<1 %

15

Duyuan Xu, Jie Xiao, Jiankun He, Weimin Wang. "Strong earthquake clustering around the eastern Tibetan Plateau after the 2008 MW7.9 Wenchuan earthquake", Science China Earth Sciences, 2020

Publication

<1 %

16

git.pyrocko.org

Internet Source

<1 %

17

M. Bernard. "Kinematics of active deformation in the Sulaiman Lobe and Range, Pakistan", Journal of Geophysical Research, 2000

Publication

<1 %

18

docplayer.net

Internet Source

<1 %

19

Bin Shan, Yong Zheng, ChengLi Liu, ZuJun Xie, Jun Kong. "Coseismic Coulomb failure stress changes caused by the 2017 M7.0 Jiuzhaigou earthquake, and its relationship with the 2008

<1 %

Wenchuan earthquake", Science China Earth Sciences, 2017

Publication

20

www.visualearth.org

Internet Source

<1 %

21

citeseerx.ist.psu.edu

Internet Source

<1 %

22

Muhammad Naseem, Shamim Ahmed Sheikh ., Shahid Naseem .. "Sedimentology of Chitarwata Formation, Rakhi Nala, Sulaiman Range, Pakistan", Journal of Applied Sciences, 2003

Publication

<1 %

23

Bin Shan, Xiong Xiong, Yong Zheng, FaQi Diao. "Stress changes on major faults caused by M w7.9 Wenchuan earthquake, May 12, 2008", Science in China Series D: Earth Sciences, 2009

Publication

<1 %

24

www.scirp.org

Internet Source

<1 %

25

Eleftheria Papadimitriou, Xueze Wen, Vassilios Karakostas, Xueshen Jin. "Earthquake Triggering along the Xianshuihe Fault Zone of Western Sichuan, China", Pure and Applied Geophysics, 2004

Publication

<1 %

26

Weilong Rao, Wenke Sun. "Moho Interface Changes Beneath the Tibetan Plateau Based on GRACE Data", Journal of Geophysical Research: Solid Earth, 2021

Publication

<1 %

27

M.A. Aurelio, J.D.B. Dianala, K.J.L. Taguibao, L.R. Pastoriza, K. Reyes, R. Sarande, A. Lucero. "Seismotectonics of the 6 February 2012 Mw 6.7 Negros Earthquake, central Philippines", Journal of Asian Earth Sciences, 2017

Publication

<1 %

28

nceg.upesh.edu.pk

Internet Source

<1 %

29

Ki-Bok Min, Jaewon Lee, Ove Stephansson. "Implications of thermally-induced fracture slip and permeability change on the long-term performance of a deep geological repository", International Journal of Rock Mechanics and Mining Sciences, 2013

Publication

<1 %

30

hdl.handle.net

Internet Source

<1 %

31

wikimili.com

Internet Source

<1 %

32

Taku Ozawa, Sou Nishimura, Yutaka Wada, Hiroshi Ohkura. "Coseismic deformation of the Mid Niigata prefecture Earthquake in 2004

<1 %

detected by RADARSAT/InSAR", Earth, Planets and Space, 2014

Publication

33

livrepository.liverpool.ac.uk

Internet Source

<1 %

34

Strong Wen, Chau-Huei Chen, Ta-Liang Teng. "Ruptures in a Highly Fractured Upper Crust", Pure and Applied Geophysics, 2012

Publication

<1 %

35

Fatih Sunbul. "Time-dependent stress increase along the major faults in eastern Turkey", Journal of Geodynamics, 2019

Publication

<1 %

36

A. Turgut, N. S. Isik, K. Ercin Kasapoglu. "A new empirical equation proposed for the relationship between surface rupture length and the earthquake source parameters", Bulletin of Engineering Geology and the Environment, 2016

Publication

<1 %

Exclude quotes On

Exclude matches Off

Exclude bibliography On